

**NASA TECHNICAL
MEMORANDUM**

NASA TM X-72843

NASA TM X-72843

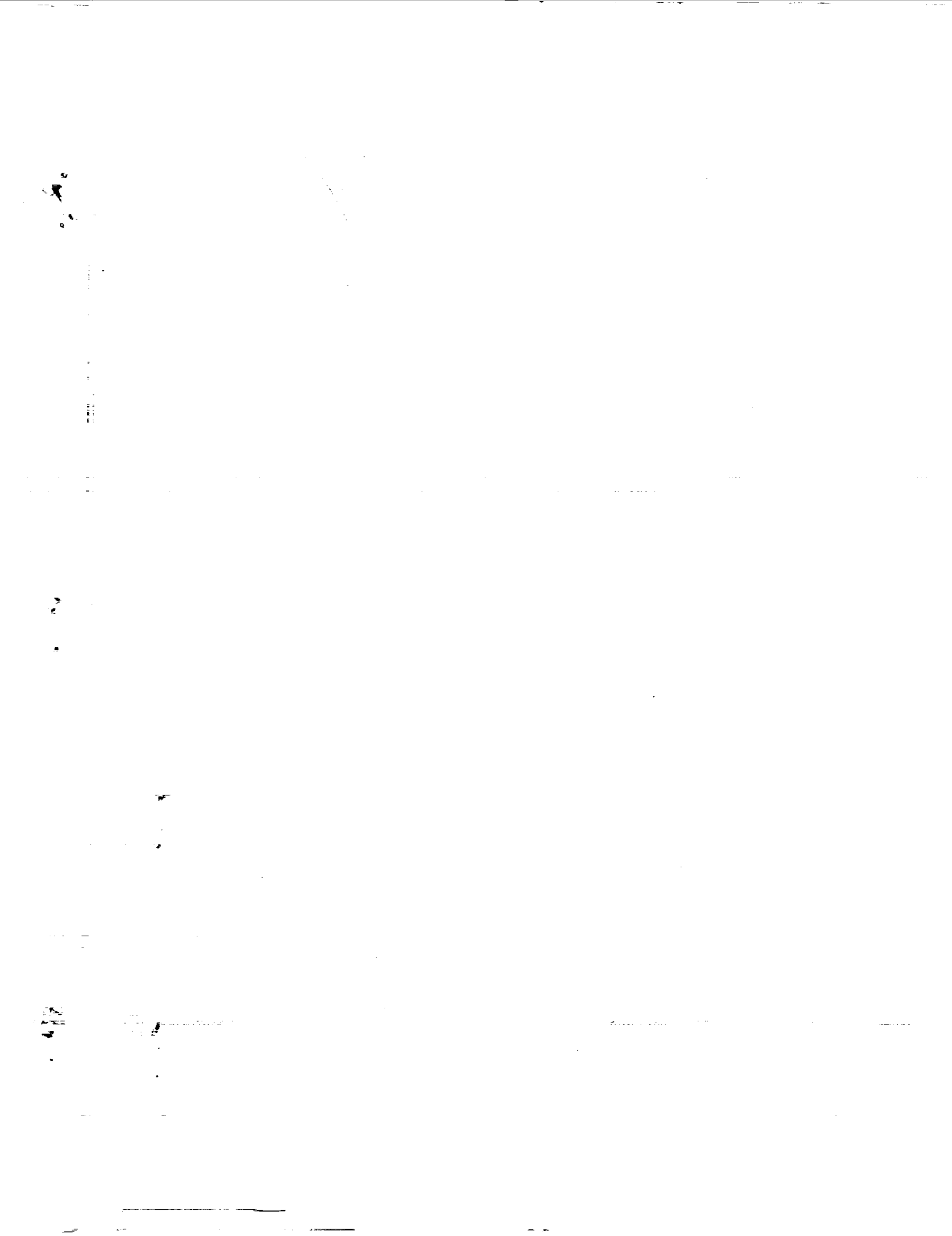
EFFECTS OF THICKNESS ON THE
AERODYNAMIC CHARACTERISTICS OF AN
INITIAL LOW-SPEED FAMILY OF AIRFOILS
FOR GENERAL AVIATION APPLICATIONS

By Robert J. McGhee and William D. Beasley

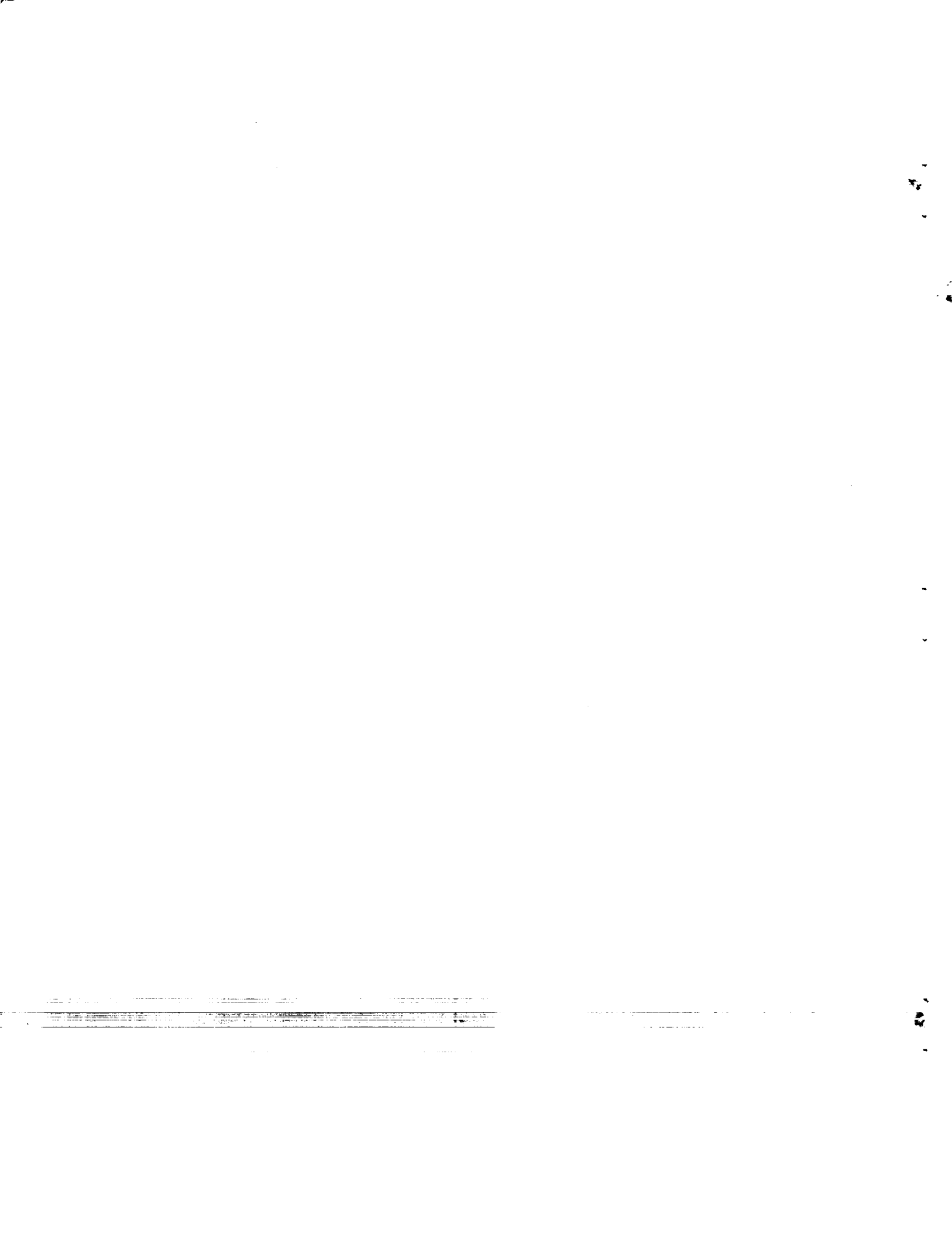
(NASA-TM-X-72843) EFFECTS OF THICKNESS ON THE AERODYNAMIC CHARACTERISTICS OF AN INITIAL LOW-SPEED FAMILY OF AIRFOILS FOR GENERAL AVIATION APPLICATIONS (NASA) 51 p
HC A04/MF A01 CACL 01A G3/02 N79-13000
Unclas 32342

REPRODUCED BY
**NATIONAL TECHNICAL
INFORMATION SERVICE**
U. S. DEPARTMENT OF COMMERCE
SPRINGFIELD, VA. 22161

**NATIONAL AERONAUTICS AND SPACE ADMINISTRATION
LANGLEY RESEARCH CENTER, HAMPTON, VIRGINIA 23665**



1. Report No. NASA TM X-72843	2. Government Accession No.	3. Recipient's Catalog No.
4. Title and Subtitle Effects of Thickness on the Aerodynamic Characteristics of an Initial Low-Speed Family of Airfoils for General Aviation Applications	5. Report Date June 1976	6. Performing Organization Code
	8. Performing Organization Report No.	10. Work Unit No. 505-06-31-02
7. Author(s) Robert J. McGhee and William D. Beasley	11. Contract or Grant No.	13. Type of Report and Period Covered Technical Memorandum
9. Performing Organization Name and Address NASA Langley Research Center Hampton, VA 23665	14. Sponsoring Agency Code	
	12. Sponsoring Agency Name and Address National Aeronautics and Space Administration Washington, DC 20546	
15. Supplementary Notes Special technical information release, planned for formal NASA publication at a later date.		
16. Abstract Wind-tunnel tests have been conducted to determine the effects of airfoil thickness-ratio on the low-speed aerodynamic characteristics of an initial family of airfoils. The family of airfoils are designated as NASA LS(1)-0413, 0417, and 0421 airfoils. The results were compared with theoretical predictions obtained from a subsonic viscous method. The tests were conducted over a Mach number range from 0.10 to 0.28. Chord Reynolds numbers varied from about 2.0×10^6 to 9.0×10^6 .		
17. Key Words (Suggested by Author(s)) (STAR category underli) General Aviation Aircraft Low-Speed Airfoil Sections Reynolds Number Effects Thickness Ratio Effects Experimental-Theoretical Comparison		
19. Security Classif. (of this report) Unclassified	20. Security Classif. (of this page) Unclassified	21. No. of Pages 22. Price



EFFECTS OF THICKNESS ON THE
AERODYNAMIC CHARACTERISTICS OF AN
INITIAL LOW-SPEED FAMILY OF AIRFOILS
FOR GENERAL AVIATION APPLICATIONS

By Robert J. McGhee and William D. Beasley

Langley Research Center

SUMMARY

An investigation was conducted in the Langley low-turbulence pressure tunnel to determine the effects of airfoil thickness ratio on the aerodynamic characteristics of an initial family of airfoils. The results are compared with theoretical predictions obtained from a subsonic viscous method. The tests were conducted over a Mach number range from about 0.10 to 0.28 and a Reynolds number range from about 2.0×10^6 to 9.0×10^6 . The geometric angle of attack varied from about -10° to 22° .

The results of the investigation indicate that the 13-percent airfoil provided the best performance for this thickness family of airfoils. At a Reynolds number of 4.0×10^6 with fixed transition near the leading edge, the maximum lift-drag ratios were about 100, 80, and 60 for the 13, 17, and 21-percent airfoils. Increasing the airfoil thickness ratio resulted in an average increase in drag coefficient of about three counts (0.0003) for each percent increase in thickness ratio at the design lift coefficient with fixed transition near the leading edge. Maximum lift coefficients at a Mach number of 0.15 and a Reynolds number of 6.0×10^6 decreased from about 2.0 to 1.8 as the airfoil thickness ratio increased from 0.13 to 0.21. Stall characteristics were of the trailing-edge type for the airfoil family. Maximum lift coefficient was generally insensitive to roughness, just sufficient to trip

the boundary-layer, for the 13-percent airfoil but was progressively more sensitive with increasing thickness ratio. Maximum lift coefficients for this thickness family were substantially greater than the older NACA airfoils of comparable thickness ratios. Comparisons of experimental section data with the theoretical viscous method of NASA CR-2523 were good for the 13- and 17-percent airfoils, but were poor for the 21-percent airfoil.

INTRODUCTION

Research on advanced technology airfoils has received considerable attention over the last several years at the Langley Research Center. References 1 and 2 report the results of 17- and 13-percent-thick airfoils designed for light General Aviation airplanes. References 3 and 4 report the results of a Fowler flap system and spoiler effectiveness for the 17-percent-thick airfoil. This report presents the basic low-speed aerodynamic characteristics of a 21-percent-thick airfoil derived from the 17-percent-thick airfoil of reference 1. In addition, this report discusses the effects of varying airfoil thickness ratio for this initial family and indicates some of the limitations in present analytical performance prediction methods.

The investigation was performed in the Langley low-turbulence pressure tunnel over a Mach number range from 0.10 to 0.28. The chord Reynolds number varied from about 2.0×10^6 to 9.0×10^6 . The geometrical angle of attack varied from about -10° to 22° .

SYMBOLS

Values are given in both SI and U.S. Customary Units. The measurements and calculations were made in the U.S. Customary Units.

C_p	pressure coefficient, $\frac{p_L - p_\infty}{q_\infty}$
c	airfoil chord, centimeters (inches)
c_c	section chord-force coefficient, $\int C_p d\left(\frac{z}{c}\right)$
c_d	section profile-drag coefficient, $\int_{\text{wake}} c'_d d\left(\frac{h}{c}\right)$
c'_d	point drag coefficient
c_l	section lift coefficient, $c_n \cos \alpha - c_c \sin \alpha$
c_{l_α}	lift-curve slope per degree
c_m	section pitching-moment coefficient about quarter-chord point, $-\int C_p \left(\frac{x}{c} - 0.25\right) d\left(\frac{x}{c}\right) + \int C_p \left(\frac{z}{c}\right) d\left(\frac{z}{c}\right)$
c_n	section normal-force coefficient, $-\int C_p d\left(\frac{x}{c}\right)$
h	vertical distance in wake profile, centimeters (inches)
l/d	section lift-drag ratio, c_l/c_d
M	free-stream Mach number
p	static pressure, N/m^2 (1b/ft ²)
q	dynamic pressure, N/m^2 (1b/ft ²)
R	Reynolds number based on free-stream conditions and airfoil chord
t	airfoil thickness, centimeters (inches)
x	airfoil abscissa, centimeters (inches)
z	airfoil ordinate, centimeters (inches)
z_c	mean line ordinate, centimeters (inches)
z_t	mean thickness, centimeters (inches)
α	geometric angle of attack, degrees

Subscripts:

L	local point on airfoil
max	maximum
0	conditions at $\alpha = 0^\circ$
∞	free-stream conditions

AIRFOIL DESIGN AND DESIGNATION

This airfoil family was obtained by linearly scaling the mean thickness distribution of the 17-percent-computer-designed airfoil of reference 1. Thus, all three airfoils have the same camber distribution and the design lift coefficient is 0.40. This method of obtaining the airfoil family was selected for two reasons: to determine the performance of a scaled family of airfoils and to validate the subsonic viscous method of reference 5 for a range of thickness ratios for aft cambered airfoils. The airfoil section shapes are shown in figure 1, and figure 2 shows the mean camber line and mean thickness distributions. Tables I, II, and III present the airfoil coordinates.

This initial family of airfoils are designated in the form LS(1)-XXXX. LS(1) indicates low-speed (1st series), the next two digits are equal to the airfoil design lift coefficient in tenths, and the last two digits are equal to the airfoil thickness in percent chord. Thus the GA(W)-1 airfoil (ref. 1) becomes LS(1)-0417 and the GA(W)-2 airfoil (ref. 2) becomes LS(1)-0413. The 21-percent-thick airfoil of this family is designated as LS(1)-0421.

MODELS, APPARATUS, AND PROCEDURE

Models

The airfoil models were constructed utilizing a metal core around which plastic fill and two thin layers of fiberglass were used to form the contour

of the airfoils. The models had chords of 61 cm (24 in.) and spans of 91.44 cm (36 in.). The models were equipped with both upper and lower surface orifices located 5.08 cm (2 in.) off the midspan. The airfoil surface was sanded in the chordwise direction with number 400 dry silicon carbide paper to provide a smooth aerodynamic finish. The model contour accuracy was generally within ± 0.10 mm (.004 in.).

Wind Tunnel

The Langley low-turbulence pressure tunnel (ref. 6) is a closed-throat, single-return tunnel which can be operated at stagnation pressures from 1 to 10 atmospheres with tunnel-empty test section Mach numbers up to 0.42 and 0.22, respectively. The maximum unit Reynolds number is about 49×10^6 per meter (15×10^6 per foot) at a Mach number of about 0.22. The tunnel test section is 91.44 cm (3 ft) wide by 228.6 (7.5 ft) high.

Hydraulically actuated circular plates provided positioning and attachment for the two-dimensional model. The plates are 101.60 cm (40 in.) in diameter, rotate with the airfoil, and are flush with the tunnel wall. The airfoil ends were attached to rectangular model attachment plates (fig. 3) and the airfoil was mounted so that the center of rotation of the circular plates was at $0.25c$ on the model reference line. The air gaps at the tunnel walls between the rectangular plates and the circular plates were sealed with flexible sliding metal seals, shown in figure 3.

Wake Survey Rake

A fixed wake survey rake (fig. 4) at the model midspan was cantilever mounted from the tunnel sidewall and located one chord length behind the trailing edge of the airfoil. The wake rake utilized total-pressure tubes,

0.1524 cm (0.060 in.) in diameter, and static-pressure tubes, 0.3175 cm (0.125 in.) in diameter. The total-pressure tubes were flattened to 0.1016 cm (0.040 in.) for 0.6096 cm (0.24 in.) from the tip of the tube. The static-pressure tubes each had four flush orifices drilled 90° apart and located 8 tube diameters from the tip of the tube and in the measurement plane of the total-pressure tubes.

Instrumentation

Measurements of the static pressures on the airfoil surfaces and the wake rake pressures were made by an automatic pressure-scanning system utilizing variable-capacitance-type precision transducers. Basic tunnel pressures were measured with precision quartz manometers. Angle of attack was measured with a calibrated digital shaft encoder operated by a pinion gear and rack attached to the circular model attachment plates. Data were obtained by a high-speed acquisition system and recorded on magnetic tape.

TESTS AND METHODS

The 0421 airfoil was tested at Mach numbers from 0.10 to 0.28 over an angle-of-attack range from about -10° to 22° . Reynolds number based on the airfoil chord was varied from about 2.0×10^6 to 9.0×10^6 . The airfoil was tested both smooth (natural transition) and with roughness located on both upper and lower surfaces at 0.075c. The roughness was sized for each Reynolds number according to reference 7. The roughness consisted of granular-type strips 0.127 cm (0.05 in.) wide, sparsely distributed, and attached to the airfoil surface with clear lacquer.

The static-pressure measurements at the airfoil surface were reduced to standard pressure coefficients and machine integrated to obtain-section normal-force and chord-force coefficients and section pitching-moment coefficients

about the quarter chord. Section profile-drag coefficient was computed from the wake-rake total and static pressures by the method reported in reference 8.

An estimate of the standard low-speed wind-tunnel boundary corrections (ref. 9) amounted to a maximum of about 2 percent of the measured coefficients and these corrections have not been applied to the data.

Testing of airfoil 0421 utilized high precision lower-range transducers to measure the wake-rake total pressures compared to the earlier testing of airfoils 0417 (ref. 1) and 0413 (ref. 2). These new transducers indicated a small difference in total pressure outside of the wake compared to the tunnel total pressure. Accounting for this pressure difference resulted in a minor change in the drag data reported in references 1 and 2. This drag adjustment has been applied to the most pertinent data of references 1 and 2 and included in this report.

PRESENTATION OF DATA

	Figure
Section characteristics for LS(1)-0413 airfoil.	5
Section characteristics for LS(1)-0417 airfoil.	6
Effect of Reynolds number on section characteristics for LS(1)-0421 airfoil.	7
Effect of Mach number on section characteristics for LS(1)-0421 airfoil.	8
Effect of Reynolds number on the chordwise pressure distributions for LS(1)-0421 airfoil.	9
Comparison of chordwise pressure distributions for LS(1) thickness family of airfoils.	10

	Figure
Effect of thickness ratio on section characteristics for LS(1) thickness family of airfoils.	11
Variation of maximum lift coefficient with Reynolds number for LS(1) thickness family of airfoils.	12
Variation of maximum lift coefficient with Mach number for LS(1) thickness family of airfoils.	13
Variation of drag coefficient with Reynolds number for LS(1) thickness family of airfoils.	14
Variation of lift-drag ratio with lift coefficient for LS(1) thickness family of airfoils.	15
Comparison of maximum lift coefficient for present LS(1) thickness family with NACA airfoils	16
Comparison of experimental and theoretical section characteristics for LS(1) thickness family of airfoils.	17

DISCUSSION

Lift.- The effects of thickness ratio on the lift characteristics are summarized in figure 11 for $M = 0.15$, $R = 4.0 \times 10^6$, and transition fixed at $x/c = 0.075$. The thickness ratio appears to have little effect on $c_{l,0}$ and the angle of zero lift for thickness ratios up to 0.17. However, for a thickness ratio of 0.21 the angle of zero lift increases by about 0.40° . The angle of zero lift is largely determined by the airfoil camber, and this increase is attributed to viscous decambering for the thick airfoil. Figure 7 shows a decrease in the angle of zero lift at the higher Reynolds numbers, a result of the thinner turbulent boundary-layers, which supports the viscous

decambering effect that occurred at low Reynolds numbers. The chordwise pressure data for $\alpha = 0^\circ$ and $R = 4.0 \times 10^6$ (fig. 10 (a)) clearly illustrate the decrease in lift coefficient that occurred for the 21-percent airfoil. The pressure data also indicate large adverse viscous effects with increasing angle of attack for the 21-percent airfoil. Figure 11 indicates a modest decrease in lift-curve-slope for the 21-percent airfoil.

The variation of maximum lift coefficient with thickness ratio ($R = 4.0 \times 10^6$; fig. 11) shows a decrease in $c_{l,max}$ for about 1.95 to 1.48 for an increase in thickness from 13- to 21-percent with transition fixed at $x/c = 0.075$. The effects of Reynolds number on $c_{l,max}$ for the thickness family both smooth and rough are shown in figure 12. Increases in Reynolds number has a large, favorable effect on $c_{l,max}$. The 13-percent airfoil displays the largest values of $c_{l,max}$ for the Reynolds numbers shown. Application of roughness at $x/c = 0.075$ resulted in small effects on $c_{l,max}$ for the 13-percent airfoil; however, large decreases occurred for the thicker airfoils. For example, for the 21-percent airfoil at $R = 6.0 \times 10^6$, roughness decreased $c_{l,max}$ by about 0.14.

Comparison of the maximum lift coefficients for this thickness family with the older NACA airfoils are shown in figure 16 at a Reynolds number of 6.0×10^6 for the airfoils smooth. The values of $c_{l,max}$ vary from about 2.0 to 1.80 for increases in thickness ratio from 0.13 to 0.21, for the present family. The largest values of $c_{l,max}$ for the older NACA airfoils were obtained for the 230 airfoil series, and varied from about 1.74 to 1.28 for increases in thickness ratio from 0.12 to 0.24. The new airfoil family represents a substantial improvement in $c_{l,max}$ compared to the older NACA airfoils. This result is important because it offers the possibility for improving the

performance of light general aviation airplanes by reducing the wing area and increasing the wing loading.

The effects of Mach number on $c_{l,max}$ for this airfoil family are shown in figure 13 at a Reynolds number of 6.0×10^6 . Increasing the Mach number results in similar decreases in $c_{l,max}$ for all three airfoils up to about $M = 0.28$. The large reduction in $c_{l,max}$ for the 13-percent airfoil at $M = 0.35$ is attributed to supercritical flow occurring near the leading edge on the upper surface of the thinner airfoil. The pressure data of figure 10(c) for $\alpha = 12^\circ$ and $M = 0.15$ illustrate the larger pressure peaks for the 13-percent airfoil compared to the thicker airfoils. Large pressure peaks and local supersonic velocities usually result in a decrease in $c_{l,max}$ with increasing Mach numbers.

The stall characteristics of this airfoil family are of the trailing-edge type. References 1 and 2 reported this result for the 17- and 13-percent airfoils and the pressure data of figure 9 show this result for the 21-percent airfoil.

Comparison of the experimental lift data with the viscous flow theory of reference 5 for a Reynolds number of 4.0×10^6 with transition fixed at $x/c = 0.075$ are shown in figure 17. As previously reported (ref. 1 and 2) the theoretical method satisfactorily predicts the lift data for angles of attack where no significant boundary-layer flow separation is present for both the 13- and 17-percent airfoils. However, figure 17(c) indicates poor agreement between experiment and theory for the 21-percent airfoil. This result is not surprising because of the extensive turbulent boundary-layer thickening and separation which occurred on the aft upper surface of the 21-percent airfoil at low Reynolds numbers. Examination of the pressure data

of figure 9 indicate separated-flow type pressure recovery on the aft upper surface of the airfoil at low angles of attack. Reference 5 indicates that for airfoils of thickness ratios of 0.18 or greater the theory generally overpredicts the lift. Theoretical calculations made at higher Reynolds numbers generally resulted in the same poor agreement.

Pitching-moment.- The variation of the quarter-chord pitching-moment coefficient at zero angle of attack with thickness ratio is presented in figure 11 for $R = 4.0 \times 10^6$ with transition fixed at $x/c = 0.075$. No effect of thickness ratio is shown for the 13- and 17-percent airfoils; however, a less negative value of $c_{m,0}$ (positive increment) is shown for the 21-percent airfoil. This result is attributed to the viscous decambering that occurred for the 21-percent airfoil at low Reynolds numbers (see discussion under lift). Comparison of the section data of figure 7(a) $R = 2.0 \times 10^6$ with 7(e) ($R = 9.0 \times 10^6$) illustrate the more negative values of $c_{m,0}$ resulting from the effective increase in camber for the thinner turbulent boundary layers at the higher Reynolds number. Comparisons of the experimental c_m data with the theory of reference 5 (fig. 17(c)) illustrate the poor agreement obtained for the 21-percent airfoil.

Drag and lift-drag ratio.- In practical general aviation application boundary-layer transition usually occurs near the leading-edge of the airfoils, a result of aerodynamic roughness caused by fabrication methods, dirt, paint erosion, or insect remains gathered in flight. Thus the discussion of the drag data is limited to fixed transition at $x/c = 0.075$. The effects of thickness ratio on c_d are consistent (increasing c_d with increasing thickness ratio) with the results reported in reference 10 for the NACA airfoils. At the design lift coefficient of 0.40 and $R = 4.0 \times 10^6$, figure 11 shows that

increasing thickness ratio results in about an average increase in c_d of three drag counts (0.0003) for each percent increase in thickness ratio. The variation of c_d with Reynolds number for the thickness family is shown in figure 14 for $c_l = 0.40$ and $c_l = 1.0$. The scale effects at $c_l = 0.40$ (fig. 14(a)) are generally consistent with flat-plate drag variations. At $c_l = 1.0$ (fig. 14(b)), the increments in drag are about the same for the Reynolds number range for the 13- and 17-percent airfoils. However, large increases in c_d are shown for the 21-percent airfoil, particularly at the low Reynolds numbers. This result is attributed to extensive turbulent boundary-layer separation on the aft upper surface of the airfoil as illustrated by the pressure data of figure 9.

Figure 15 shows the variation of lift-drag ratio with c_l for the thickness family. As expected, increasing the airfoil thickness decreases the lift-drag ratio, while increases in Reynolds number has a favorable effect on lift-drag ratio. At a Reynolds number of 4.0×10^6 the maximum lift-drag ratios were 100, 80, and 60 for the 13, 17, and 21-percent airfoils. Also, the lift coefficients for high lift-drag ratios were increased as the airfoil-thickness ratio was decreased.

Comparison of the experimental drag data with the theory of reference 5 (fig. 17) indicate surprisingly good agreement for the entire thickness family at lift coefficients where attached flow was present.

SUMMARY OF RESULTS

Low-speed wind-tunnel tests have been conducted in the Langley low-turbulence pressure tunnel to determine the effects of airfoil thickness ratio on the aerodynamic characteristics of an initial family of airfoils. The

results have been compared with theoretical predictions obtained from a subsonic viscous method. The tests were conducted over a Mach number range from about 0.10 to 0.28 and a Reynolds number range from about 2.0×10^6 to 9.0×10^6 . The following results were determined from this investigation:

1. The 13-percent airfoil provided the best performance for this thickness family of airfoils.
2. At a Reynolds number of 4.0×10^6 with fixed transition near the leading edge, the maximum lift-drag ratios were about 100, 80, and 60 for the 13-, 17-, and 21-percent airfoils.
3. Increasing the airfoil thickness ratio resulted in an average increase in drag coefficient of about three counts (0.0003) for each percent increase in thickness ratio at the design-lift coefficient with fixed transition near the leading edge.
4. Maximum lift coefficients at a Mach number of 0.15 and a Reynolds number of 6.0×10^6 decreased from about 2.0 to 1.8 as the airfoil thickness ratio increased from 0.13 to 0.21. Stall characteristics were of the trailing-edge type for this airfoil family.
5. Maximum lift coefficient was insensitive to roughness, just sufficient to trip the boundary layer, for the 13-percent airfoil but was progressively more sensitive with increasing thickness ratio.

6. Maximum lift coefficients for this thickness family were substantially greater than the older NACA airfoils of comparable thickness ratios.
7. Comparisons of experimental section data with the theoretical viscous method of NASA CR-2523 were good for attached boundary-layers for the 13- and 17-percent airfoils, but were poor for the 21-percent airfoil.

REFERENCES

1. McGhee, Robert J.; and Beasley, William D.: Low-Speed Aerodynamic Characteristics of a 17-Percent-Thick Airfoil Section Designed for General Aviation Applications. NASA TN D-7428, 1973.
2. McGhee, Robert J.; Beasley, William D.; and Somers, Dan M.: Low-Speed Aerodynamic Characteristics of a 13-Percent-Thick Airfoil Section Designed for General Aviation Applications. NASA TM X-72697, 1975.
3. Wentz, W. H., Jr.; and Seetharam, H. C.: Development of a Fowler Flap System for a High Performance General Aviation Airfoil. NASA CR-2443, 1974.
4. Wentz, W. H., Jr.: Effectiveness of Spoilers on the GA(W)-1 Airfoil With a High Performance Fowler Flap. NASA CR-2538, 1975.
5. Smetana, Frederick O.; Summey, Delbert C.; Smith, Neill S.; and Carden, Ronald K.: Light Aircraft Lift, Drag, and Moment Predictions - A Review and Analysis. NASA CR-2523, 1975.
6. Von Doenhoff, Albert E.; and Abbott, Frank T., Jr.: The Langley Two-Dimensional Low-Turbulence Pressure Tunnel. NACA TN 1283, 1947.

7. Braslow, Albert L.; and Knox, Eugene C.: Simplified Method for Determination of Critical Height of Distributed Roughness Particles for Boundary-Layer Transition at Mach Numbers From 0 to 5. NACA TN 4363, 1958.
8. Pankhurst, R. C.; and Holder, D. W.: Wind Tunnel Technique. Sir Isaac Pitman and Sons, Ltd., London, 1965.
9. Pope, Alan; and Harper, John J.: Low-Speed Wind-Tunnel Testing. John Wiley and Sons, Inc., New York, 1966.
10. Abbott, Ira H.; and Von Doenhoff, Albert E.: Theory of Wing Sections, Dover Publications, Inc., New York, 1959.

TABLE I.- LS(1)-0413 AIRFOIL DESIGN COORDINATES

x/c	(z/c) _{upper}	(z/c) _{lower}
0.0	0.0	0.0
.0020	.01035	-.00495
.0050	.01588	-.00935
.0125	.02424	-.01448
.0250	.03325	-.01907
.0375	.03966	-.02226
.0500	.04476	-.02498
.0750	.05261	-.02938
.1000	.05862	-.03281
.1250	.06347	-.03562
.1500	.06755	-.03792
.1750	.07103	-.03982
.2000	.07399	-.04139
.2500	.07861	-.04368
.3000	.08182	-.04484
.3500	.08381	-.04516
.4000	.08464	-.04474
.4500	.08435	-.04353
.5000	.08293	-.04144
.5500	.08023	-.03810
.5750	.07834	-.03589
.6000	.07605	-.03334
.6250	.07335	-.03051
.6500	.07024	-.02745
.6750	.06674	-.02425
.7000	.06287	-.02097
.7250	.05868	-.01767
.7500	.05419	-.01441
.7750	.04946	-.01126
.8000	.04450	-.00831
.8250	.03933	-.00568
.8500	.03397	-.00347
.8750	.02843	-.00181
.9000	.02275	-.00080
.9250	.01692	-.00058
.9500	.01096	-.00135
.9750	.00483	-.00336
1.0000	-.00156	-.00714

ORIGINAL PAGE IS
OF POOR QUALITY

TABLE II.- LS(1)-0417 AIRFOIL DESIGN COORDINATES

x/c	$(z/c)_{upper}$	$(z/c)_{lower}$
0.0	0.0	0.0
.0020	.01300	-.00974
.0050	.02035	-.01444
.0125	.03069	-.02051
.0250	.04165	-.02691
.0375	.04974	-.03191
.0500	.05600	-.03569
.0750	.06561	-.04209
.1000	.07309	-.04700
.1250	.07909	-.05087
.1500	.08413	-.05426
.1750	.08849	-.05700
.2000	.09209	-.05926
.2500	.09778	-.06265
.3000	.10169	-.06448
.3500	.10409	-.06517
.4000	.10500	-.06483
.4500	.10456	-.06344
.5000	.10269	-.06091
.5500	.09917	-.05683
.5750	.09674	-.05396
.6000	.09374	-.05061
.6250	.09013	-.04678
.6500	.08604	-.04265
.6750	.08144	-.03830
.7000	.07639	-.03383
.7250	.07096	-.02930
.7500	.06517	-.02461
.7750	.05913	-.02030
.8000	.05291	-.01587
.8250	.04644	-.01191
.8500	.03983	-.00852
.8750	.03313	-.00565
.9000	.02639	-.00352
.9250	.01965	-.00248
.9500	.01287	-.00257
.9750	.00604	-.00396
1.0000	-.00074	-.00783

TABLE III.- LS(1)-0421 AIRFOIL DESIGN COORDINATES

x/c	$(z/c)_{upper}$	$(z/c)_{lower}$
0.0	0.0	0.0
.0020	.01560	-.01071
.0050	.02377	-.01775
.0125	.03599	-.02653
.0250	.04912	-.03522
.0375	.05853	-.04137
.0500	.06606	-.04650
.0750	.07771	-.05463
.1000	.08664	-.06097
.1250	.09388	-.06612
.1500	.09993	-.07038
.1750	.10507	-.07393
.2000	.10943	-.07690
.2500	.11617	-.08130
.3000	.12074	-.08381
.3500	.12344	-.08484
.4000	.12439	-.08455
.4500	.12365	-.08288
.5000	.12112	-.07970
.5500	.11657	-.07452
.5750	.11342	-.07104
.6000	.10965	-.06701
.6250	.10525	-.06247
.6500	.10025	-.05752
.6750	.09470	-.05226
.7000	.08865	-.04678
.7250	.08216	-.04117
.7500	.07530	-.03553
.7750	.06814	-.02994
.8000	.06075	-.02456
.8250	.05318	-.01953
.8500	.04550	-.01500
.8750	.03775	-.01112
.9000	.03000	-.00805
.9250	.02232	-.00598
.9500	.01476	-.00515
.9750	.00735	-.00589
1.0000	.00016	-.00886

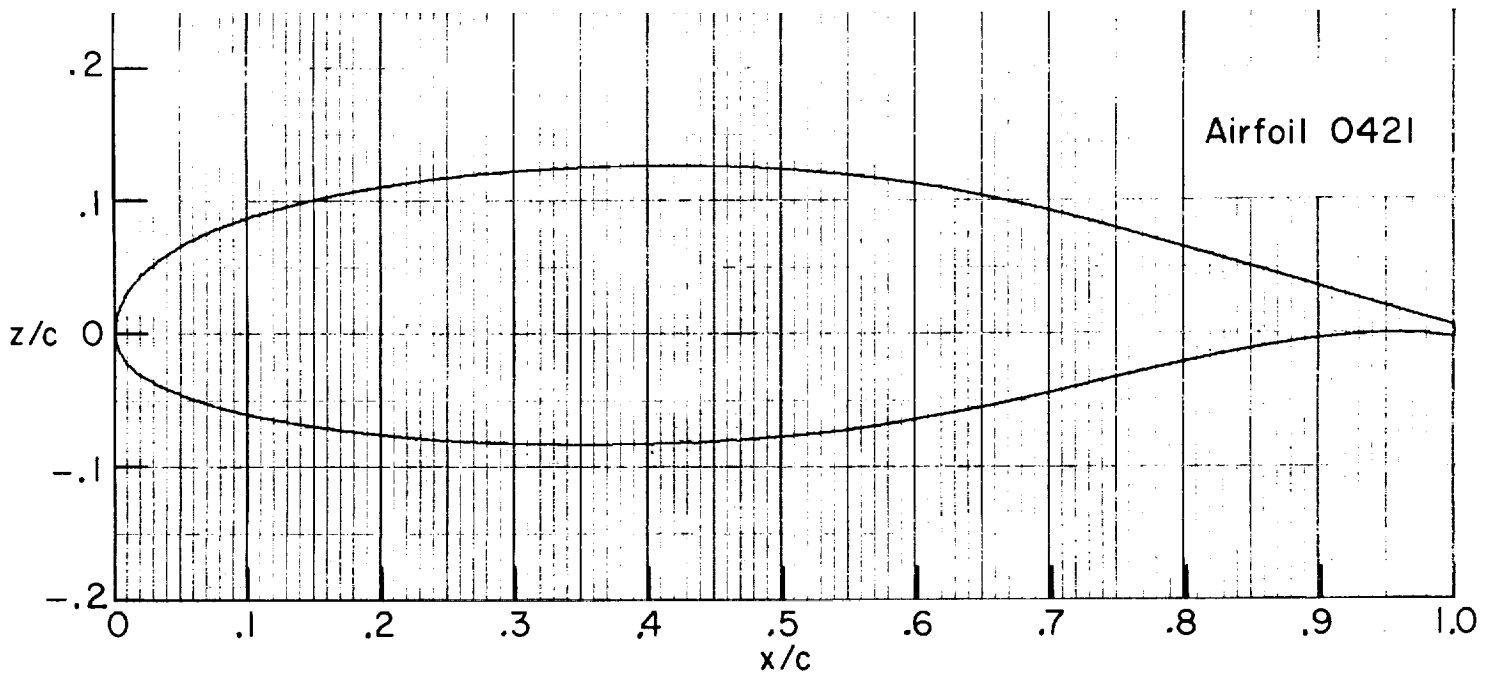
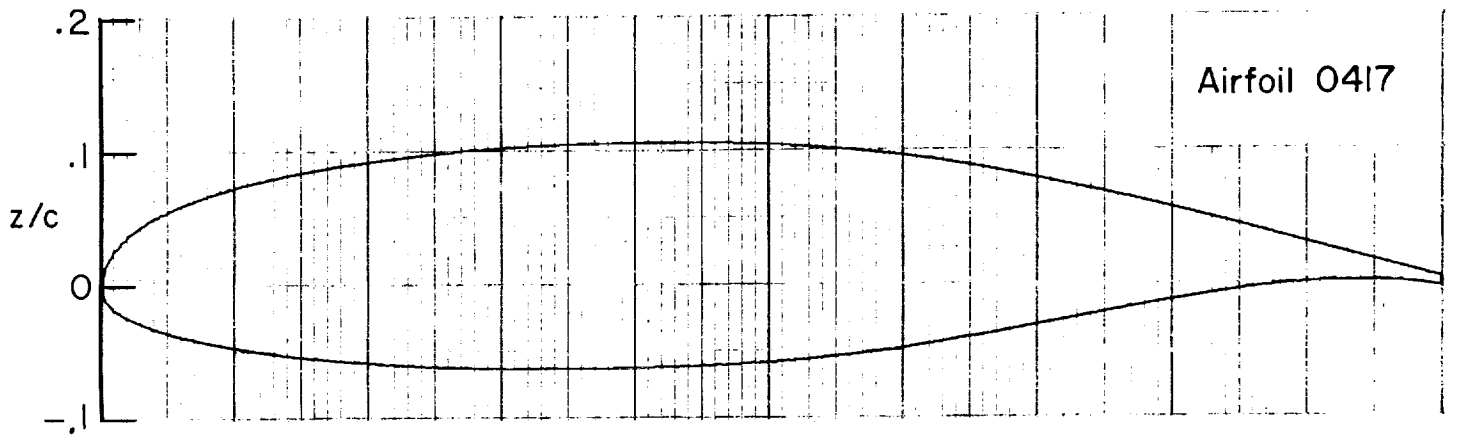
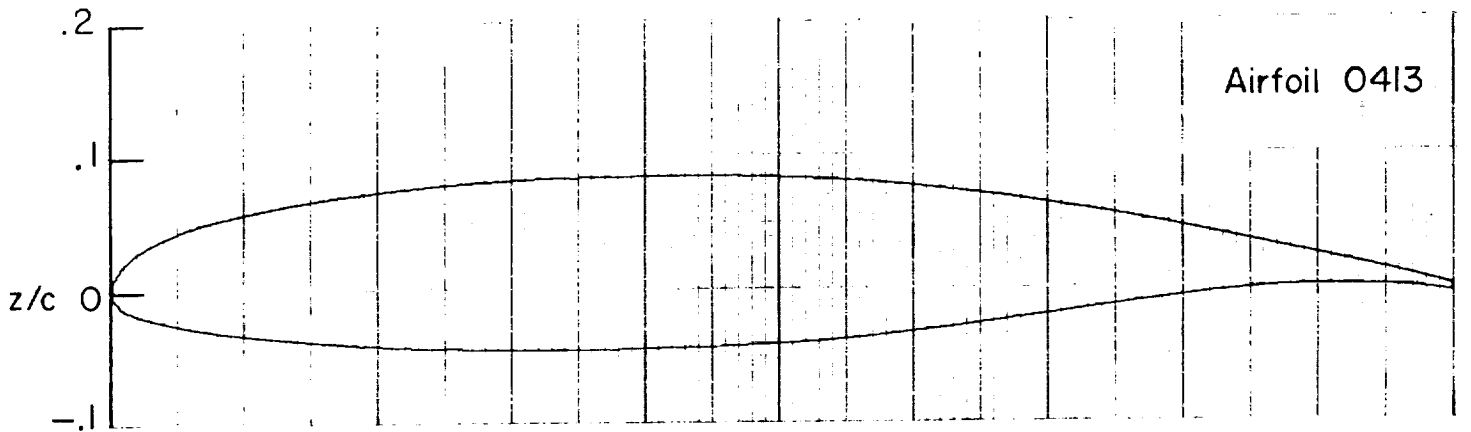


Figure 1. - Section shapes for NASA LS(l)-thickness family of airfoils.

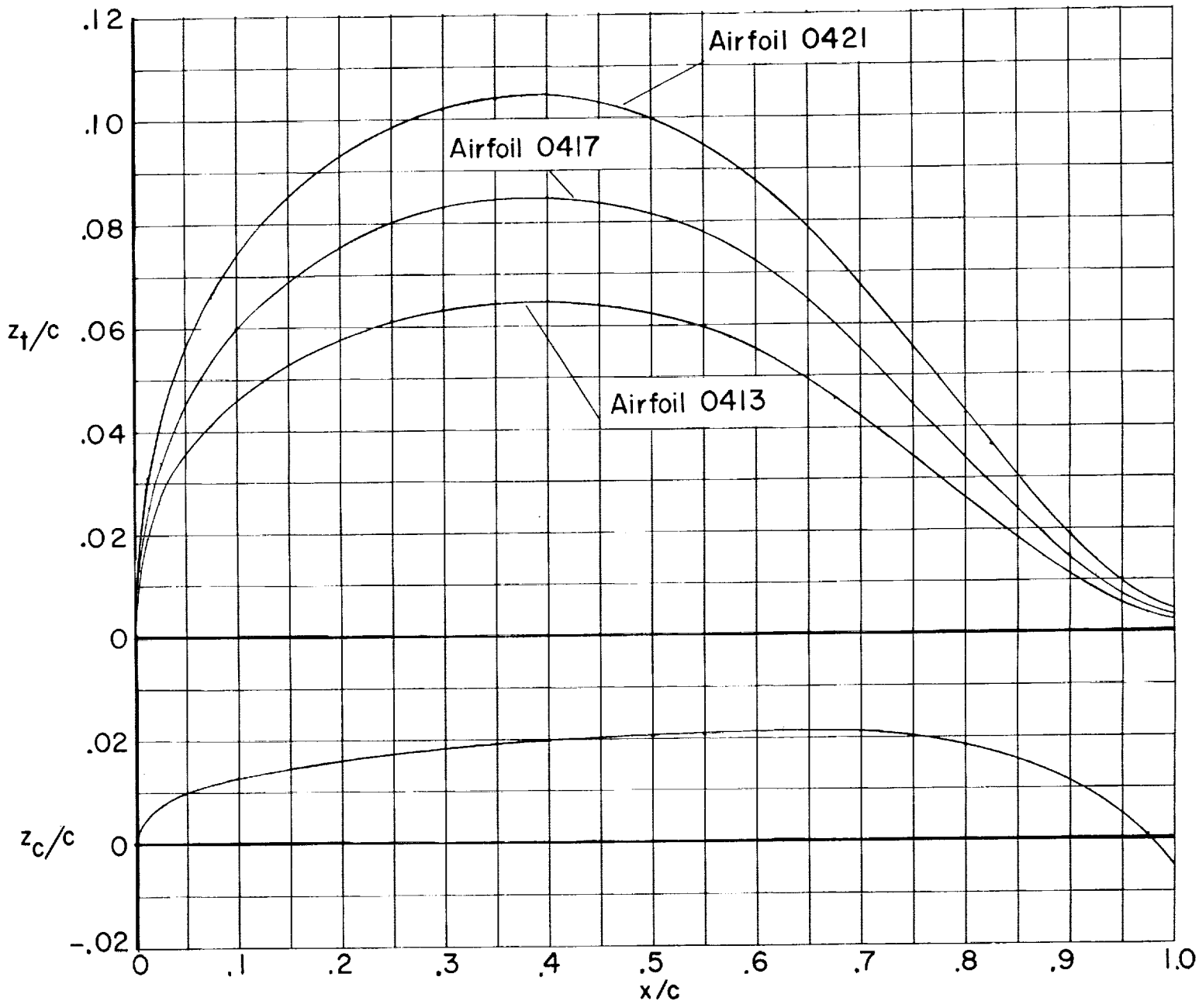


Figure 2. - Mean thickness distributions and camber line for NASA LS(1)-thickness family of airfoils.

ORIGINAL PAGE IS
OF POOR QUALITY

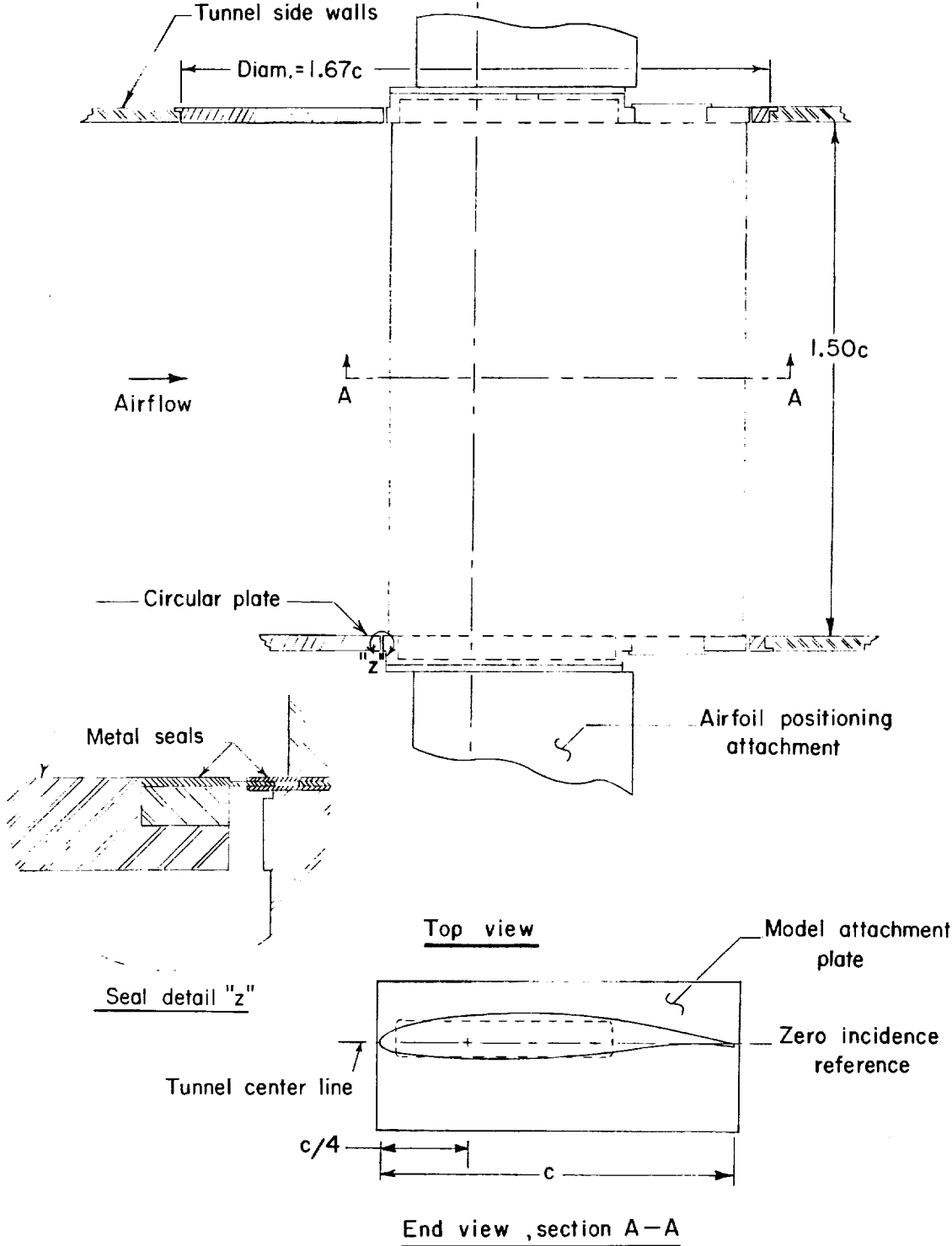


Figure 3. - Airfoil mounted in wind tunnel. All dimensions in terms of airfoil chord. $c = 61$ cm (24 in.).

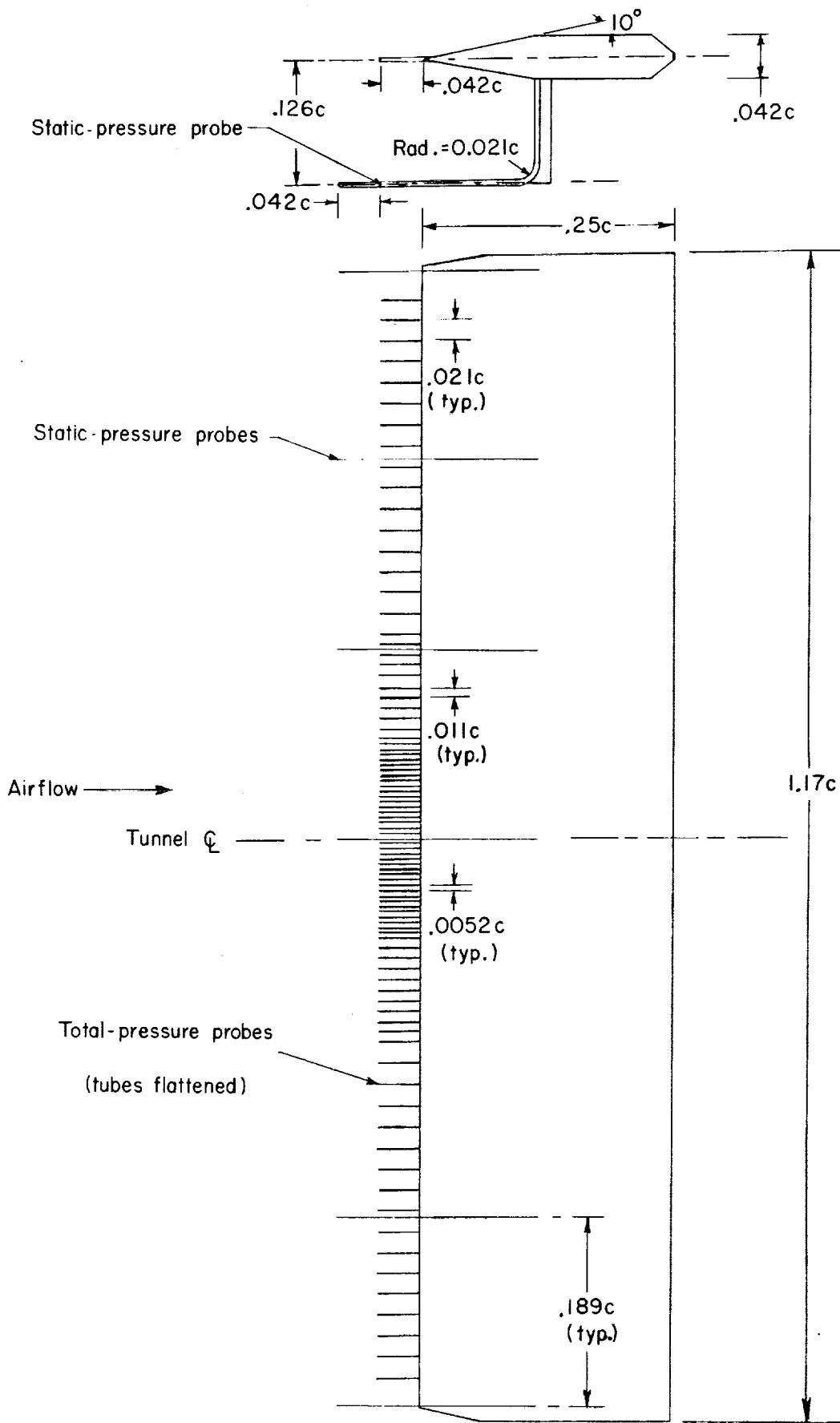


Figure 4. - Drawing of wake rake. All dimensions in terms of airfoil chord. $c = 61 \text{ cm (24 in.)}$.

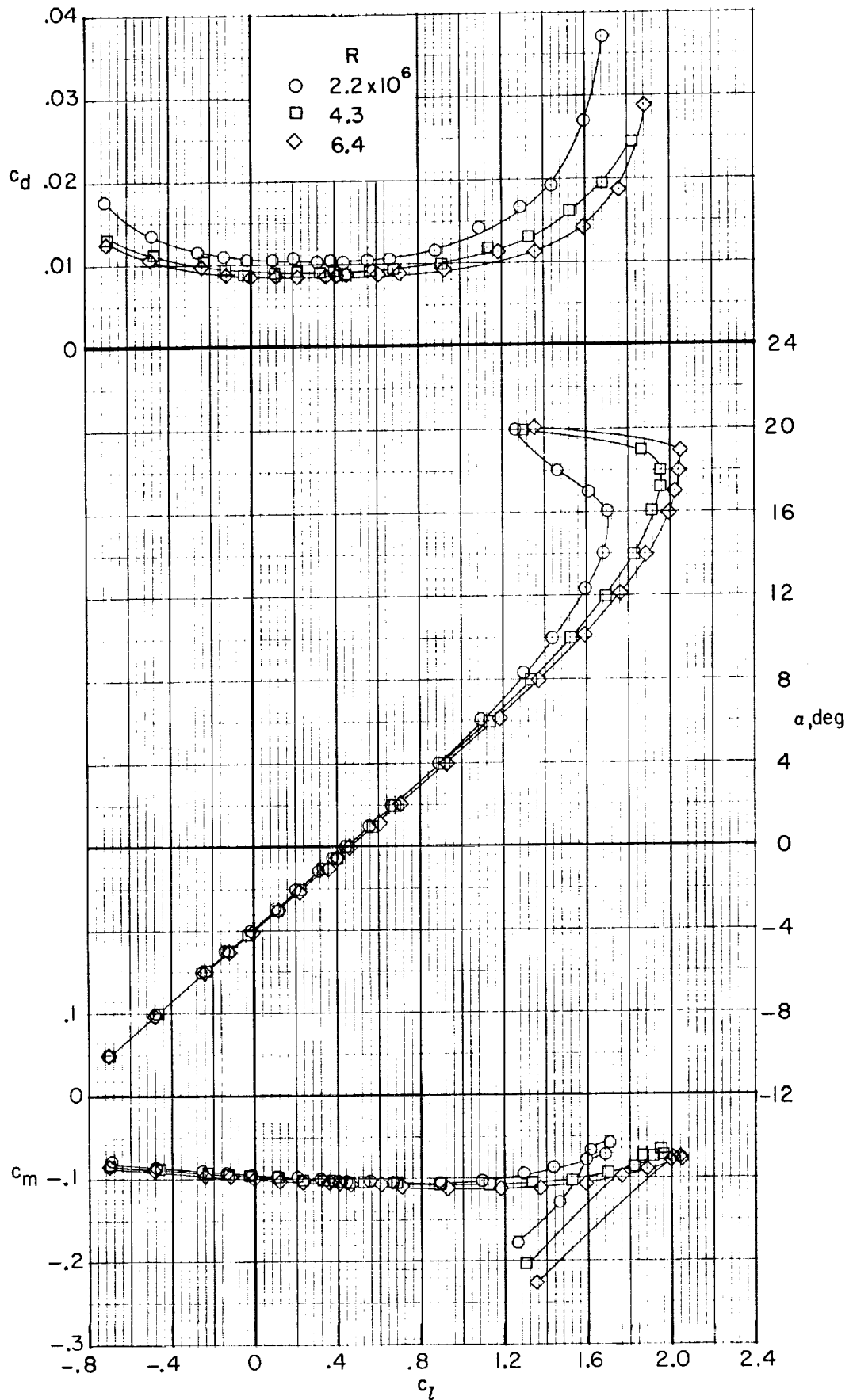


Figure 5. - Section characteristics for LS(1)-0413 airfoil. $M = 0.15$; transition fixed at $x/c = 0.075$.

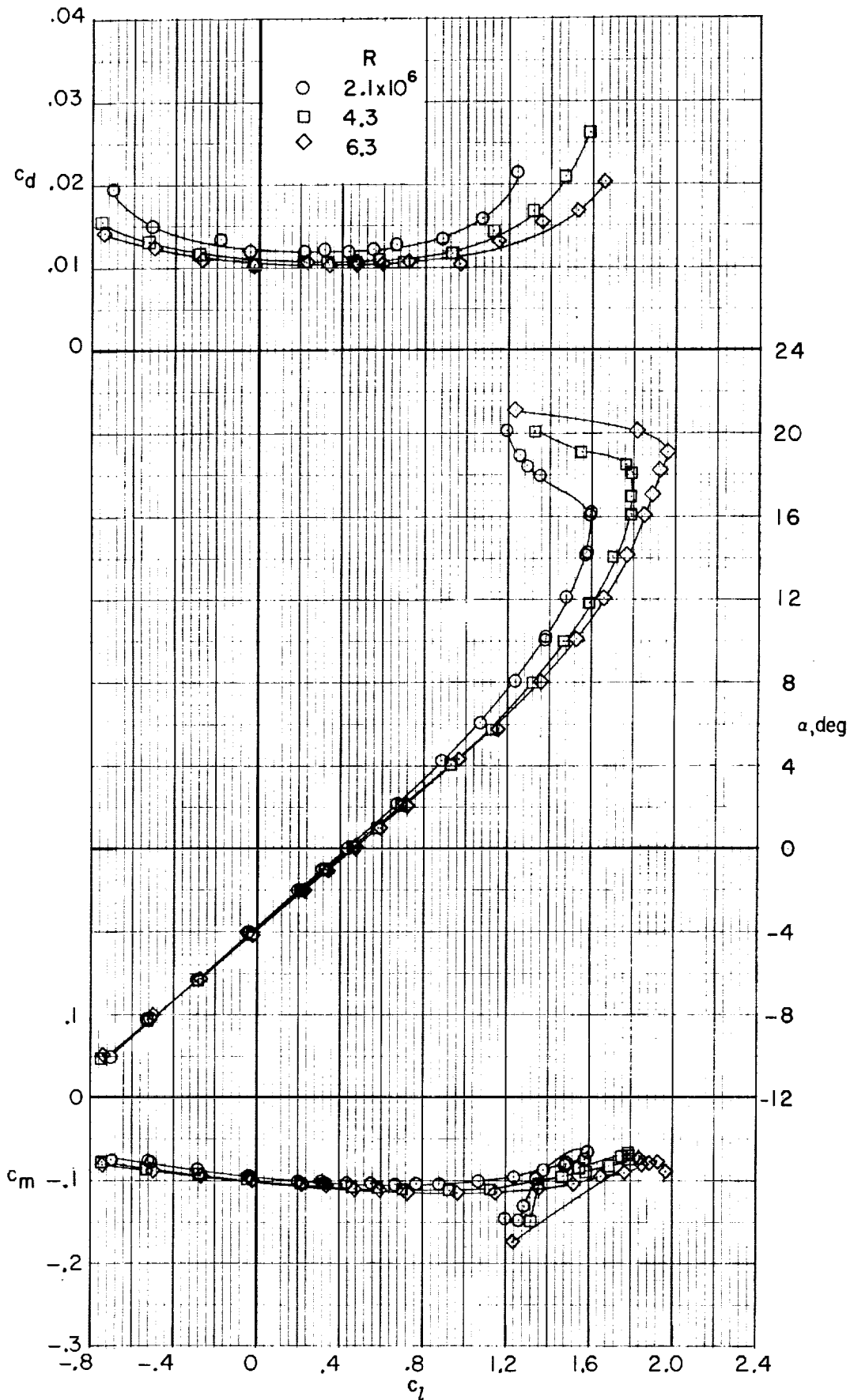
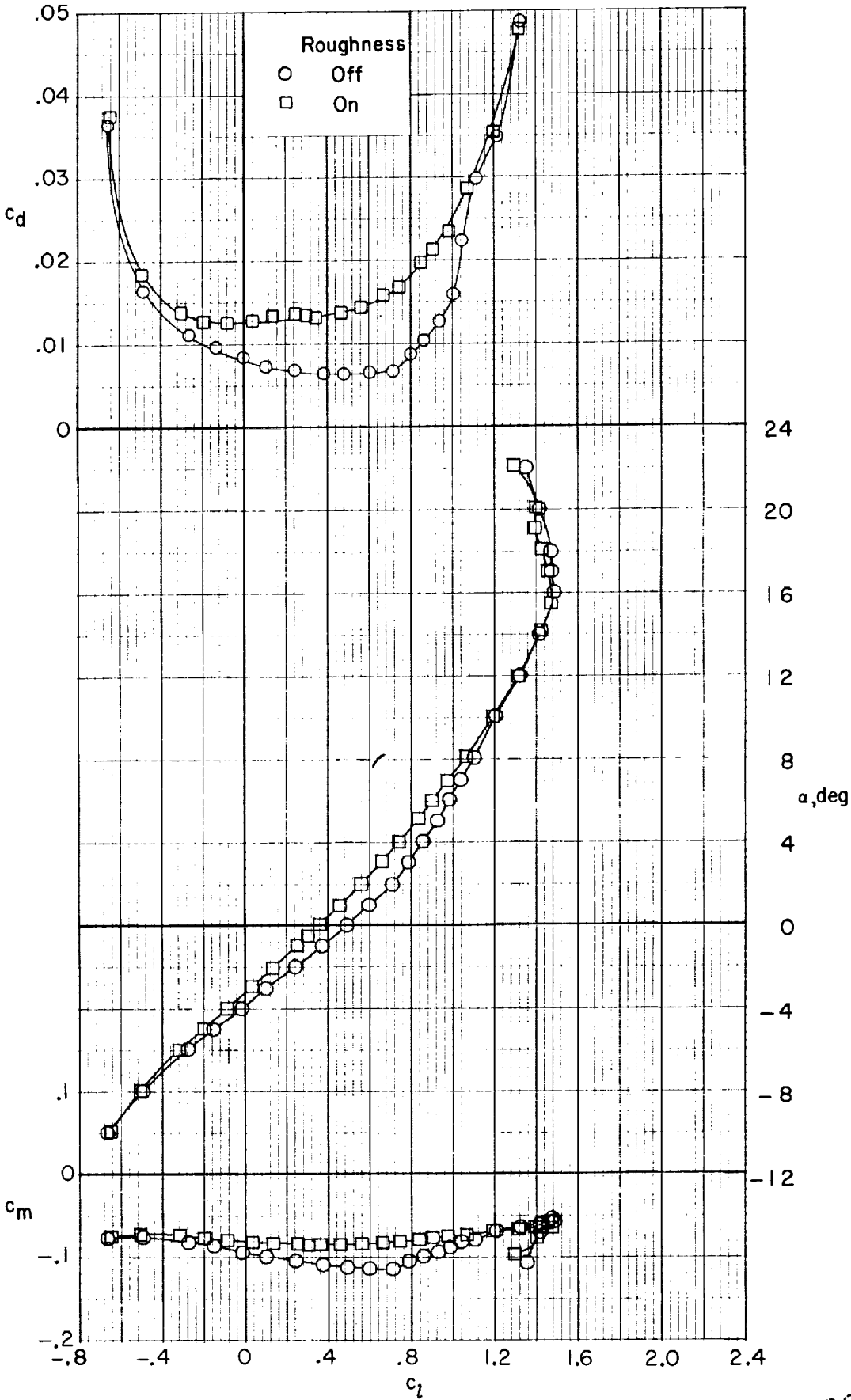
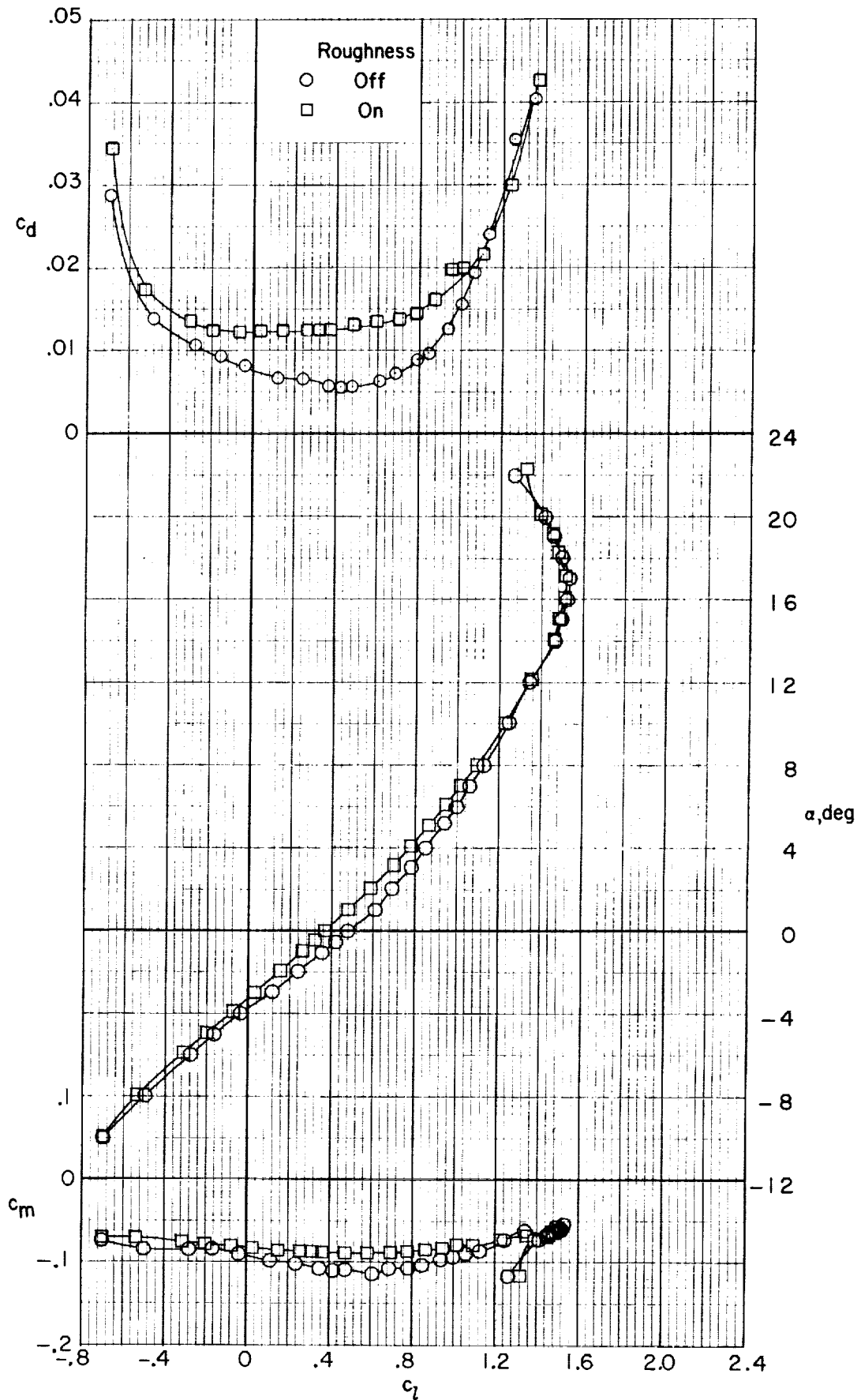


Figure 6. - Section characteristics for LS(1)-0417 airfoil. $M = 0.15$; transition fixed at $x/c = 0.075$.



(a) $R \approx 2.0 \times 10^6$.

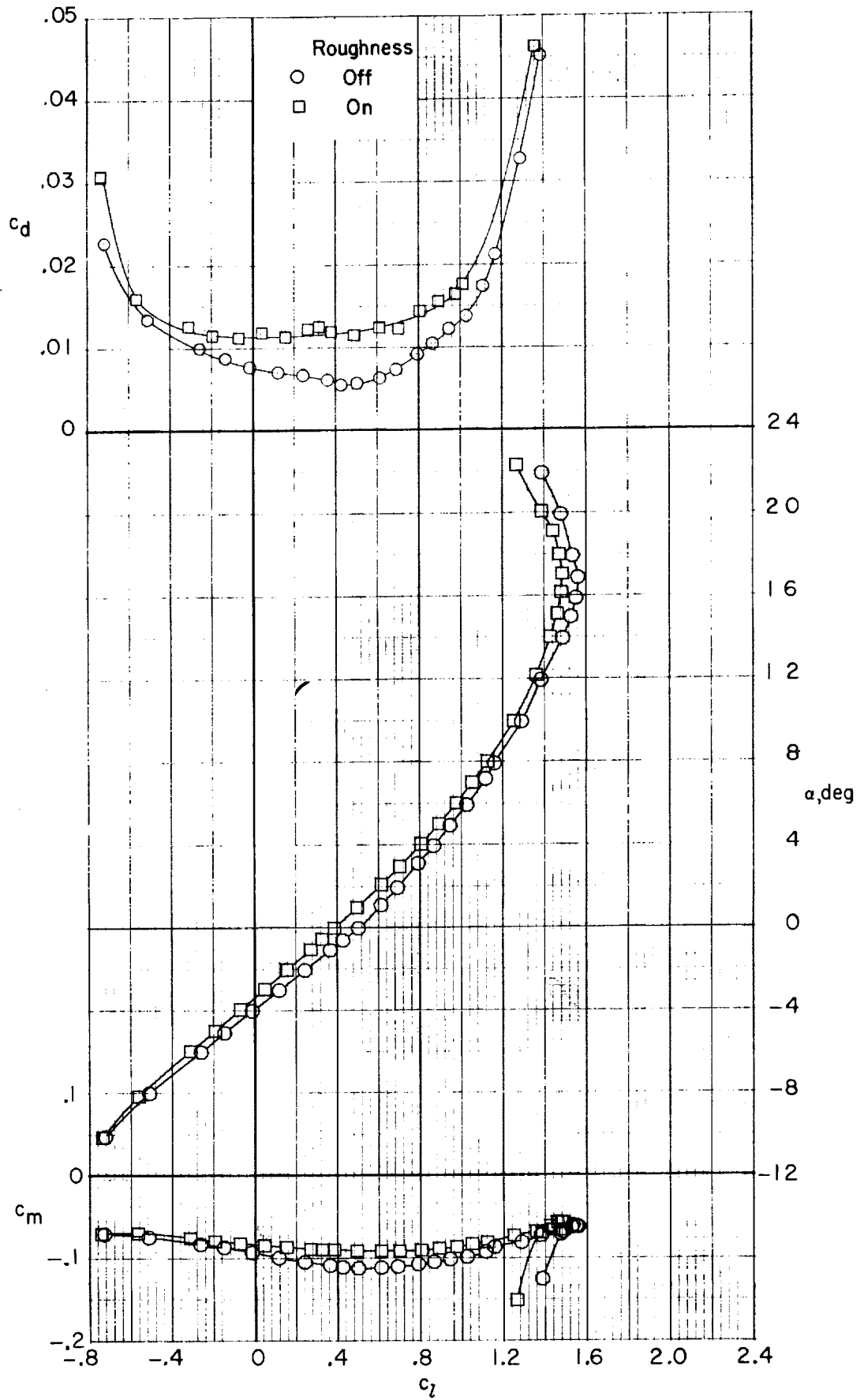
Figure 7. - Effect of Reynolds number on section characteristics for LS(1)-0421 airfoil.
 $M = 0.15$.



(b) $R \approx 3.0 \times 10^6$.

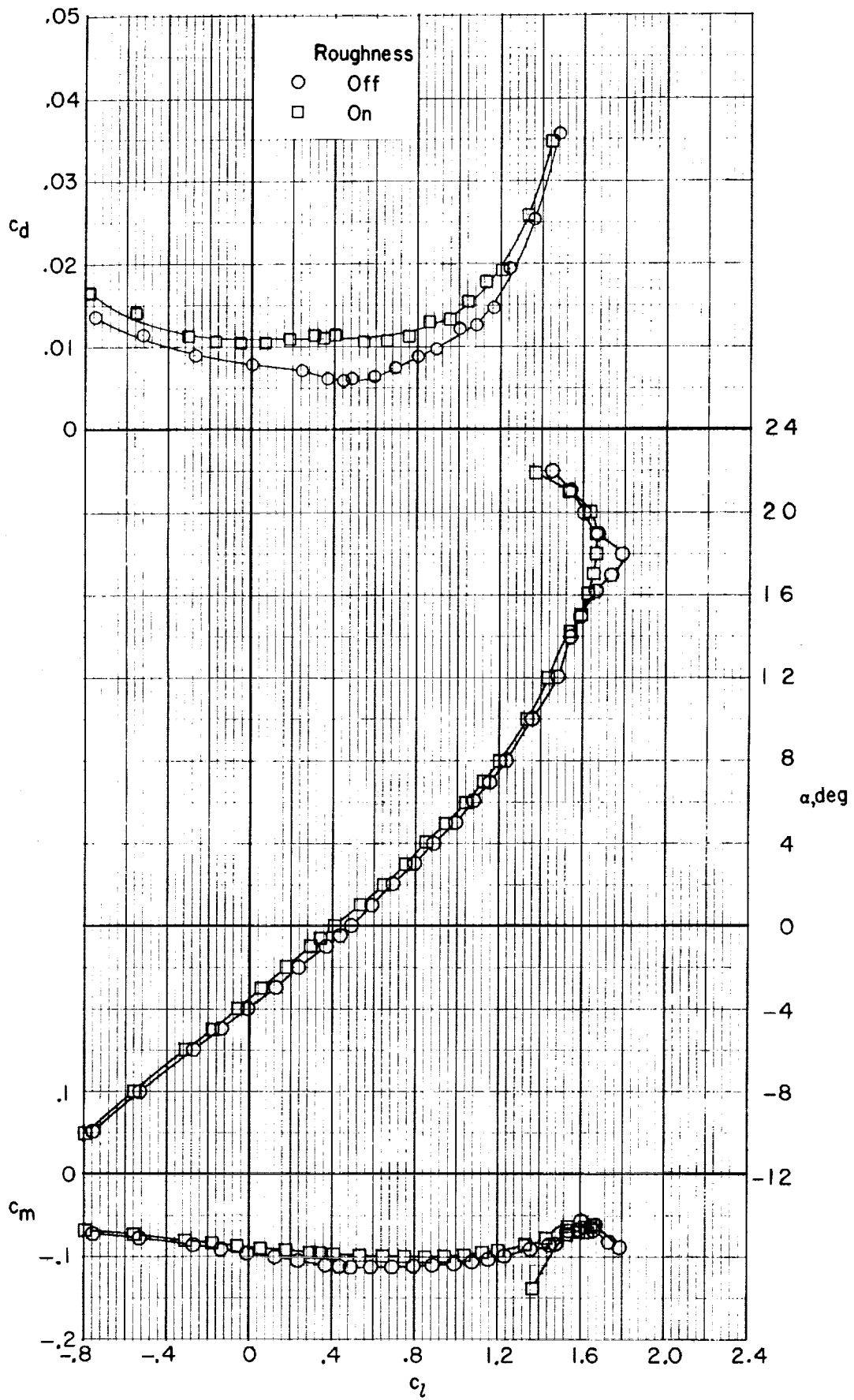
Figure 7. - Continued.

26



(c) $R \approx 4.0 \times 10^6$.

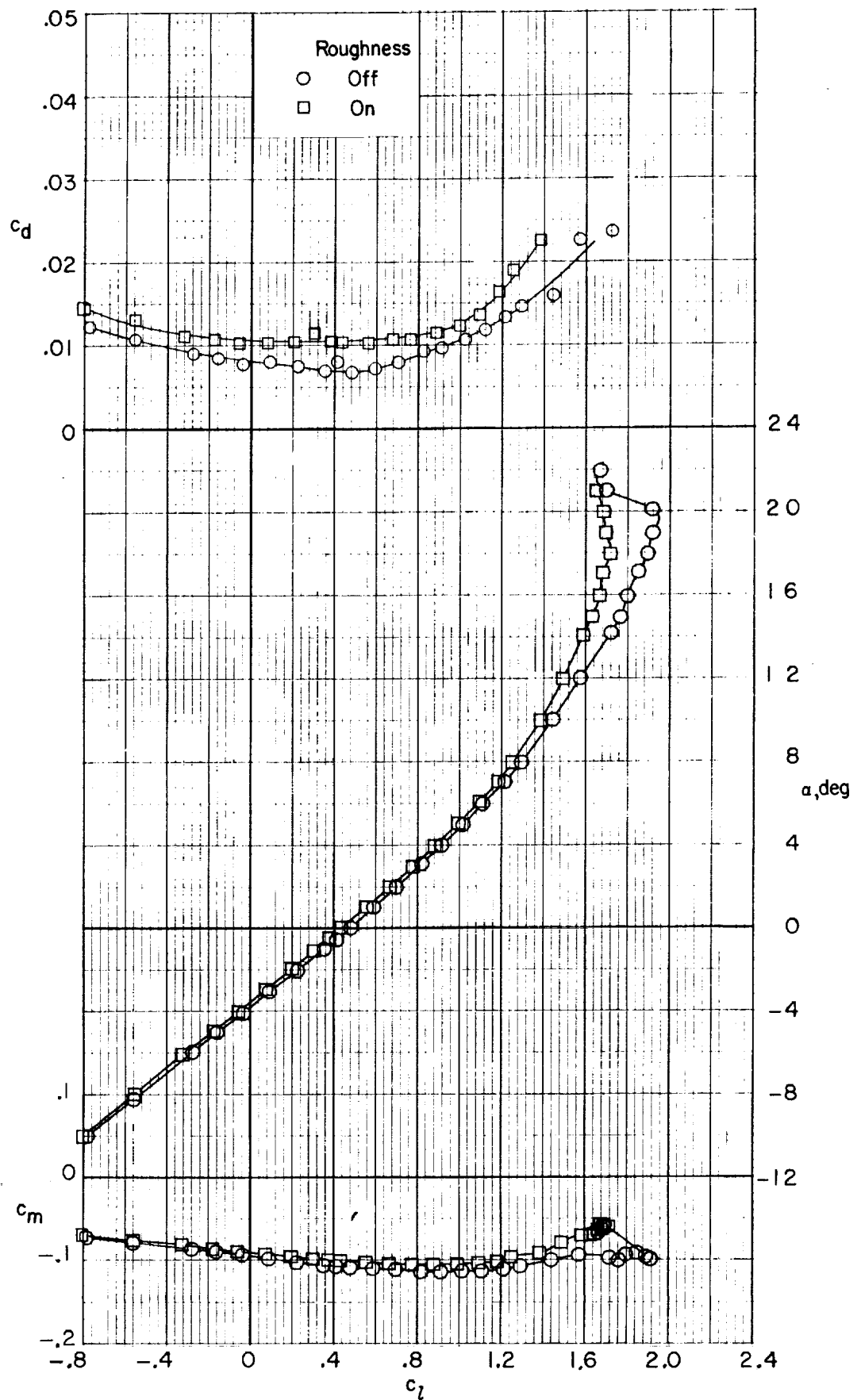
Figure 7. - Continued.



28

(d) $R \approx 6.0 \times 10^6$.

Figure 7. - Continued.



(e) $R \approx 9.0 \times 10^6$.

Figure 7. - Concluded.

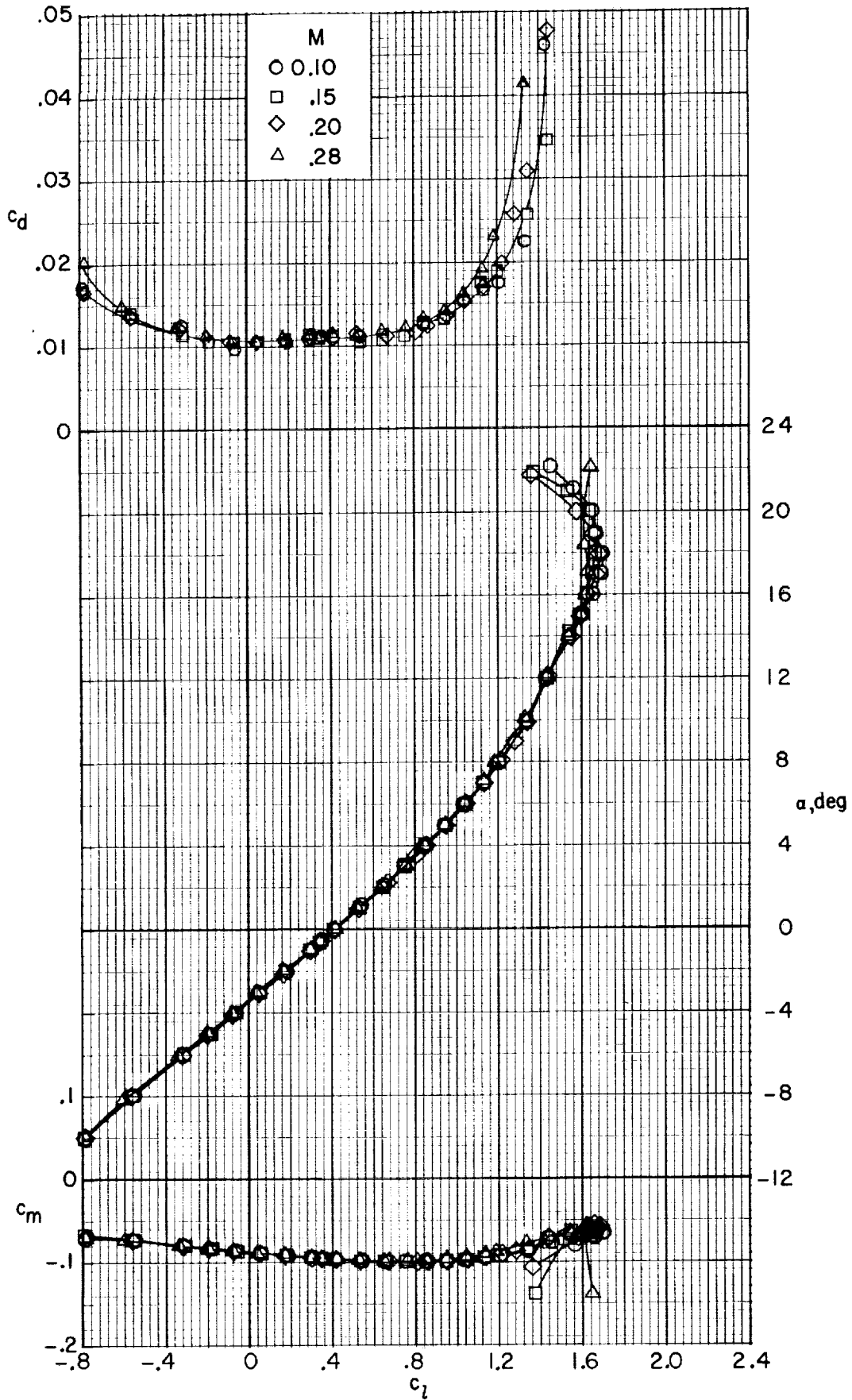
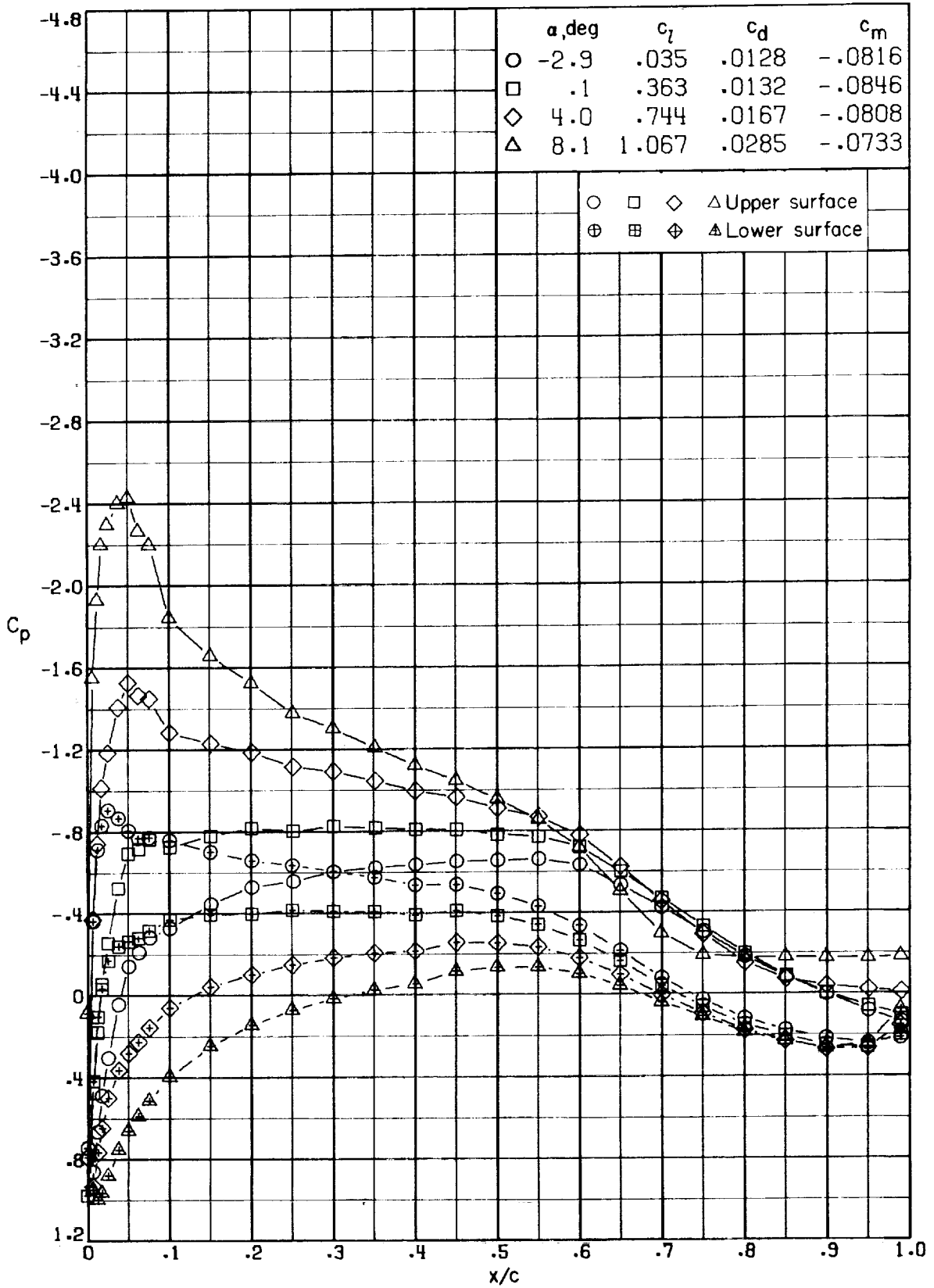
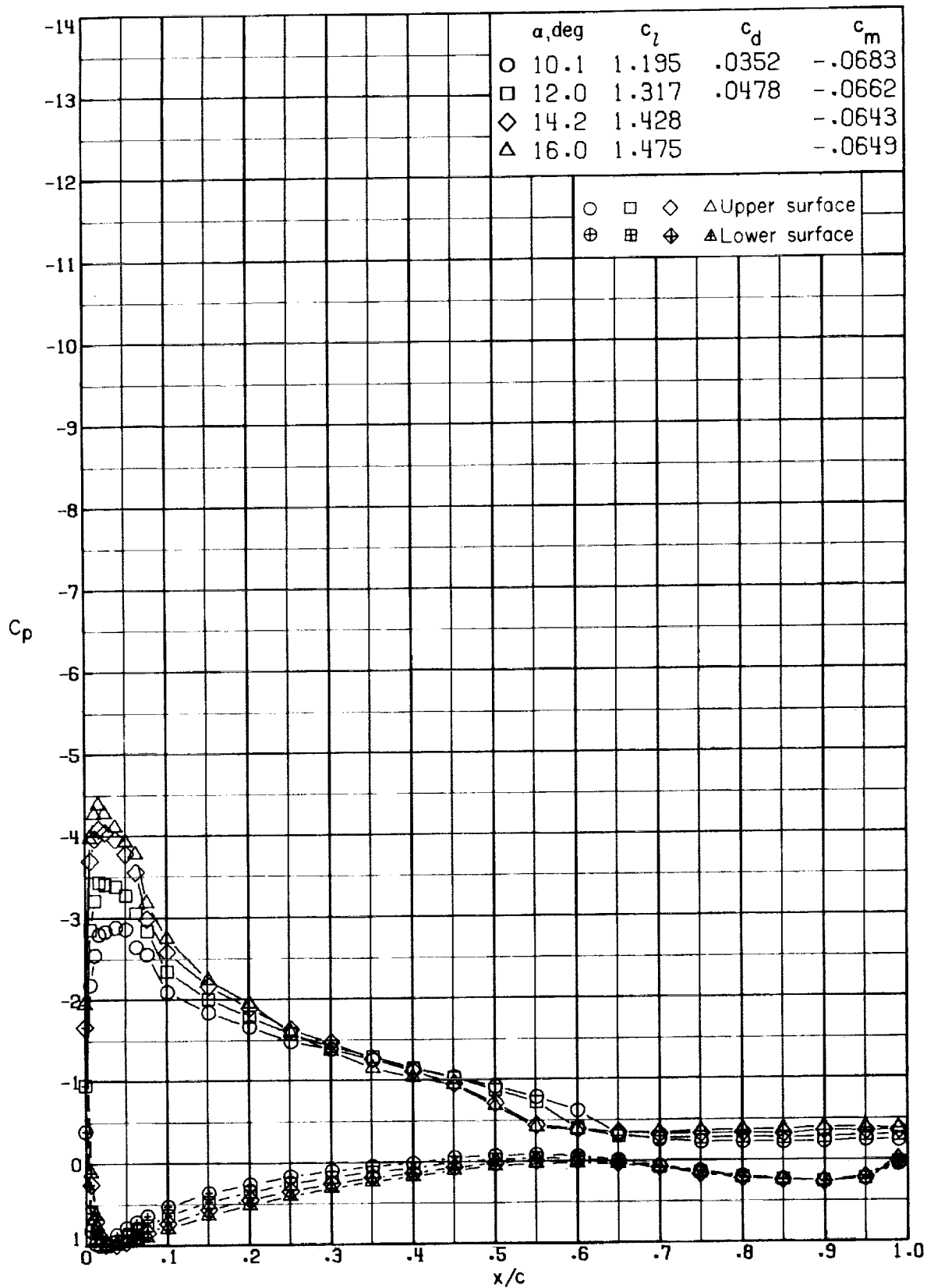


Figure 8. - Effect of Mach number on section characteristics for LS(1)-0421 airfoil.
 $R \approx 6.0 \times 10^6$; transition fixed at $x/c = 0.075$.



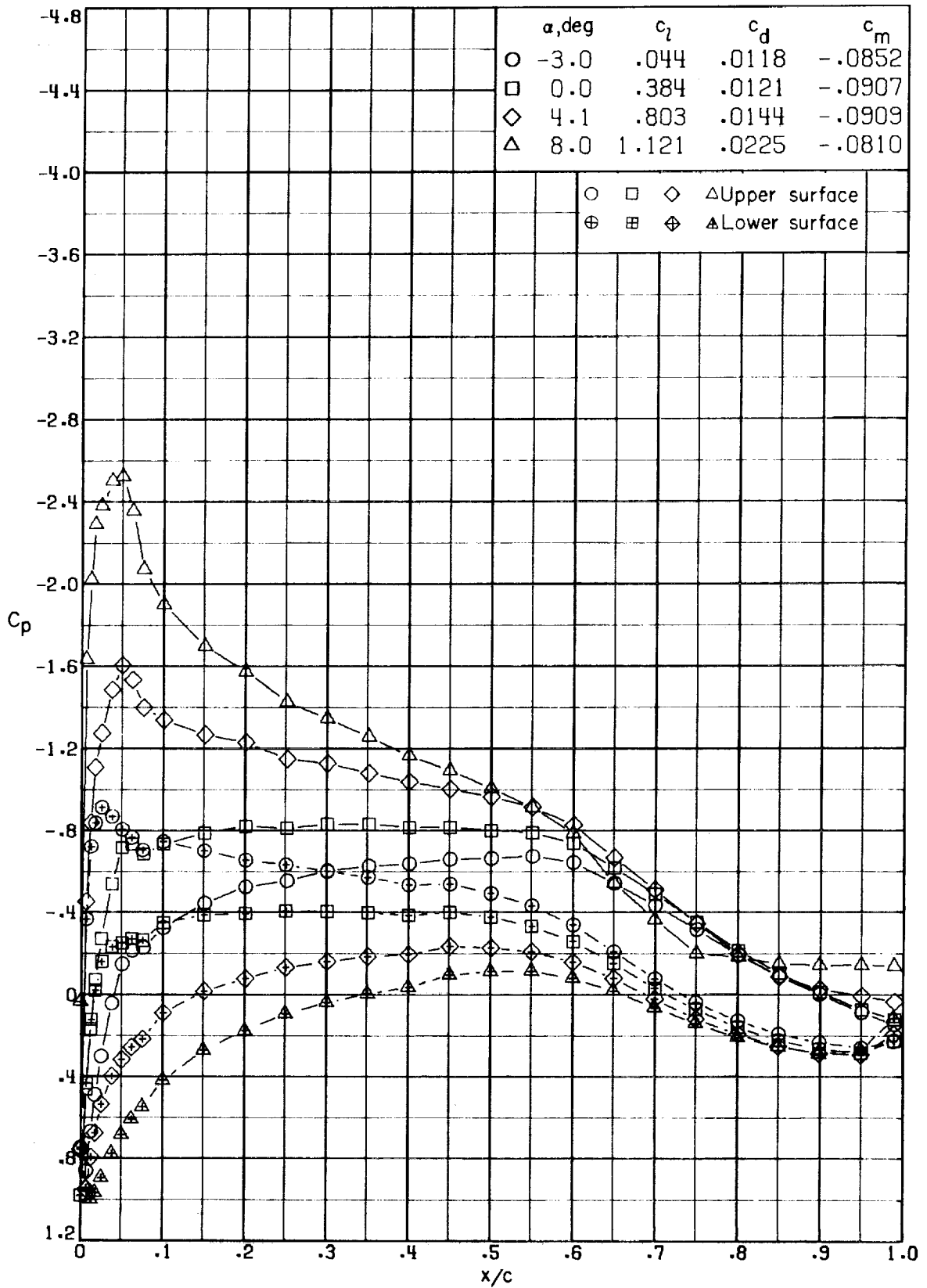
(a) $R = 2.1 \times 10^6$.

Figure 9. - Effect of Reynolds number on chordwise pressure distributions for LS(1)-0421 airfoil.
 $M = 0.15$; transition fixed at $x/c = 0.075$.



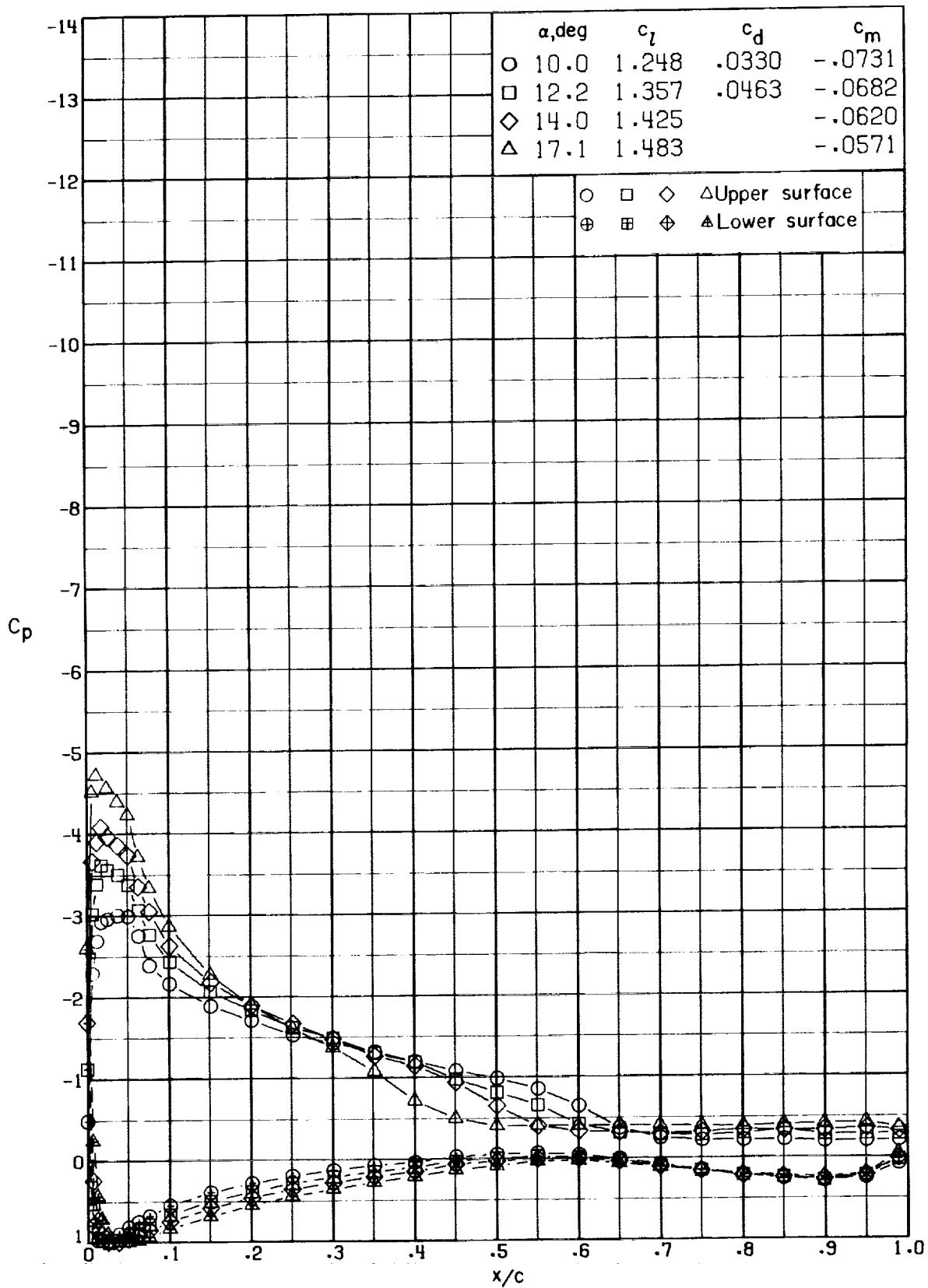
(a) $R = 2.1 \times 10^6$. Concluded.

Figure 9. - Continued.



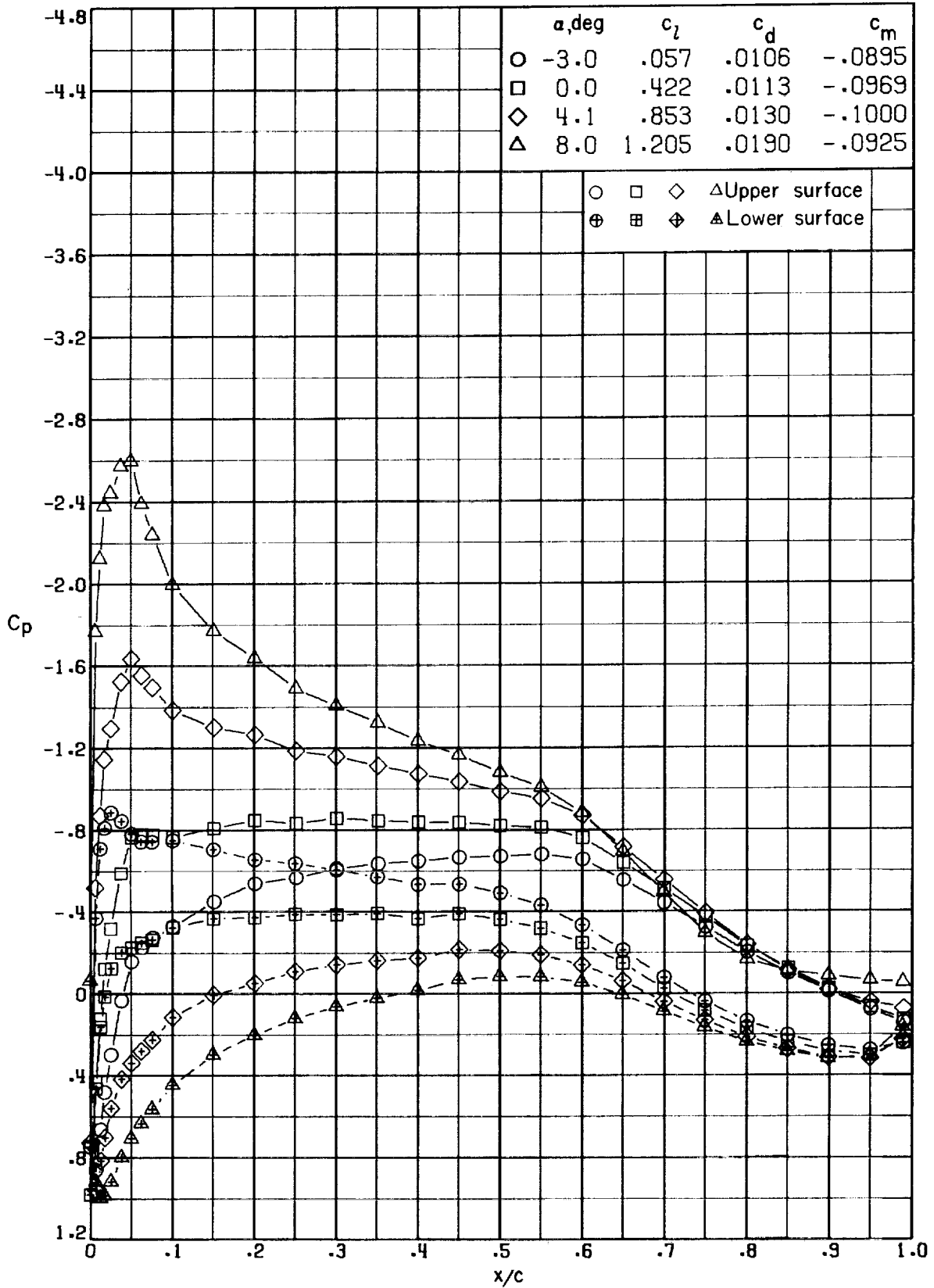
(b) $R = 3.9 \times 10^6$.

Figure 9. - Continued.



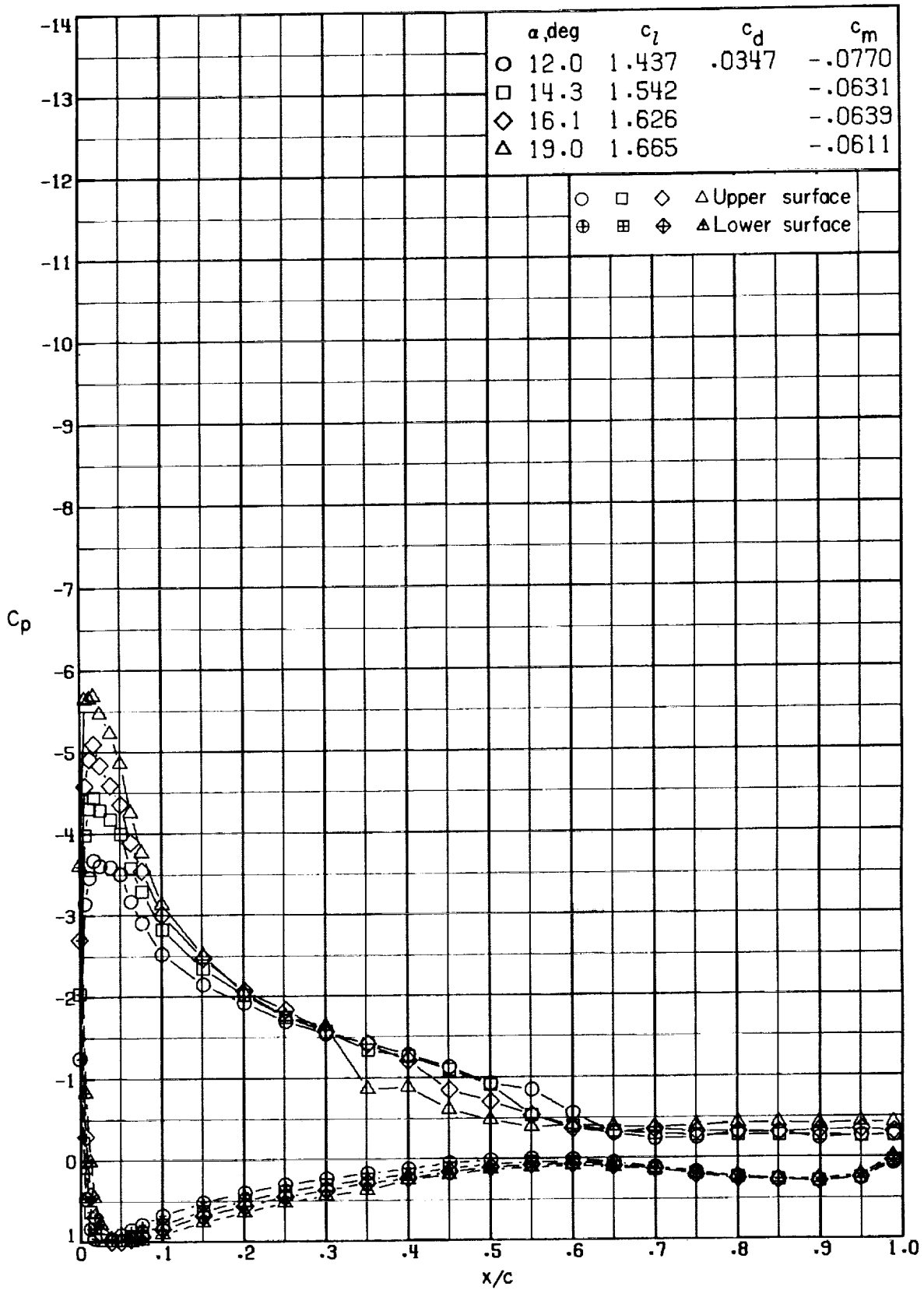
(b) $R = 3.9 \times 10^6$. Concluded.

Figure 9. - Continued.



(c) $R = 6.0 \times 10^6$.

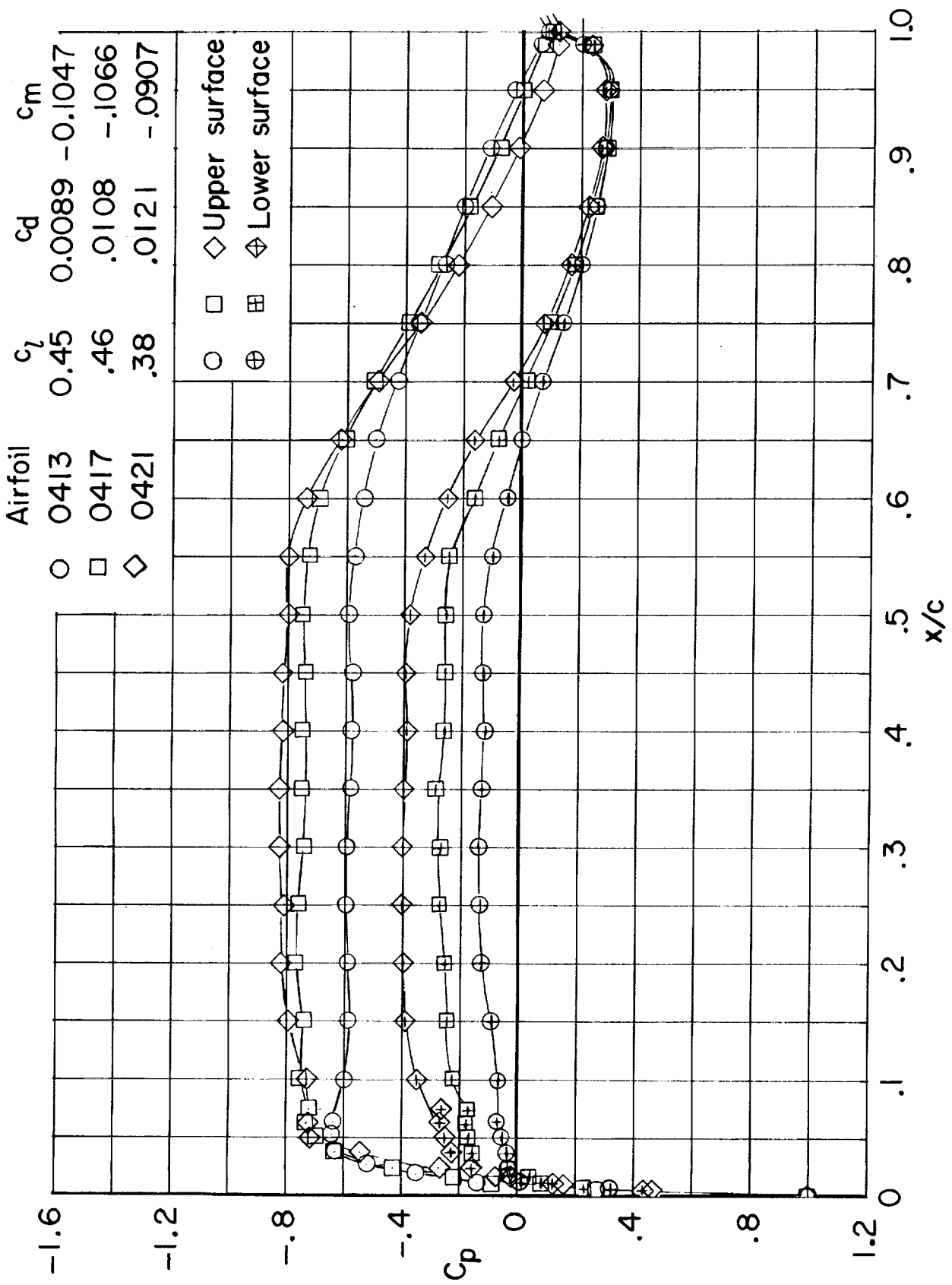
Figure 9. - Continued.



(c) $R = 6.0 \times 10^6$, Concluded.

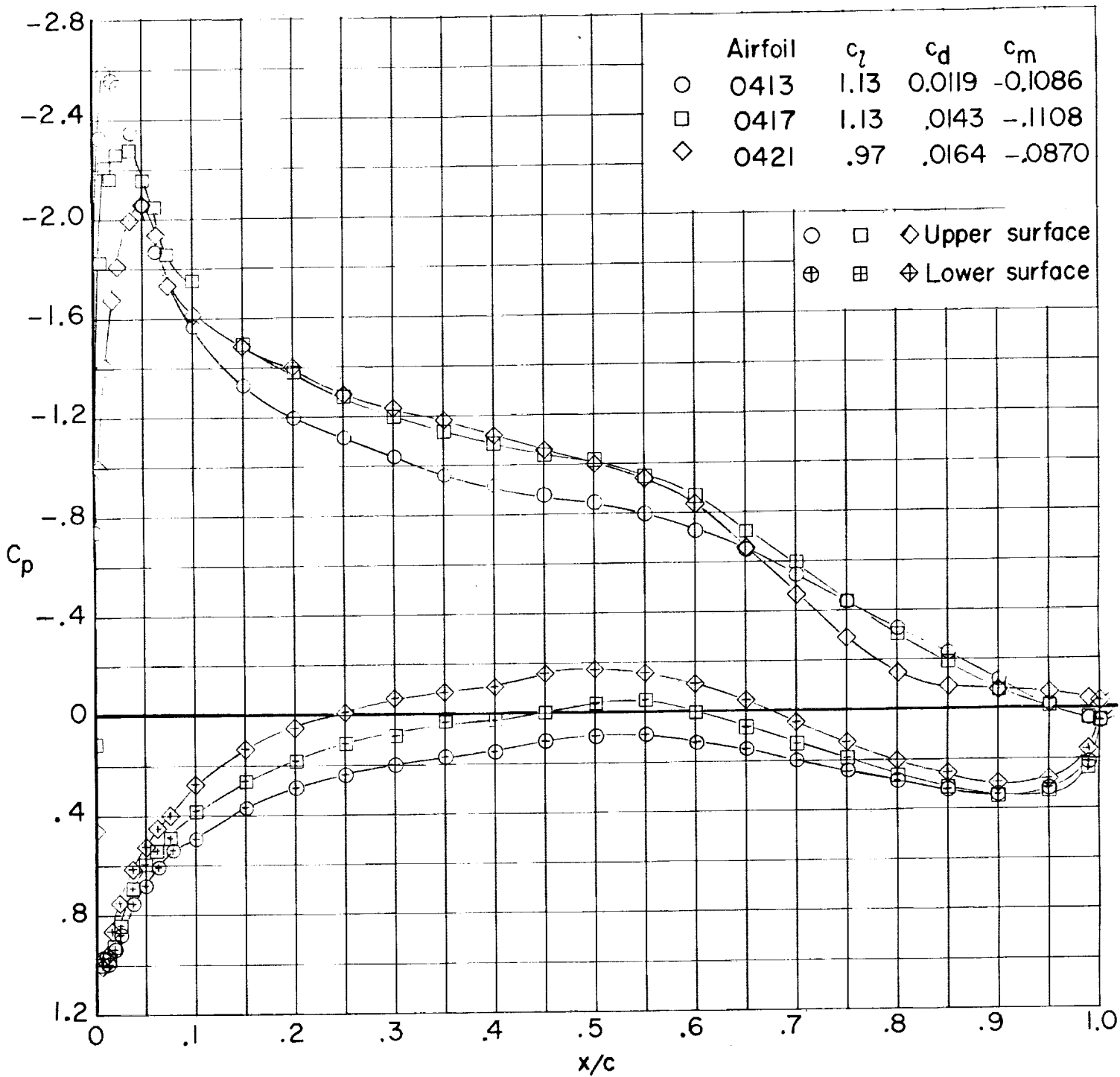
Figure 9. - Concluded.

ORIGINAL PAGE IS
OF POOR QUALITY



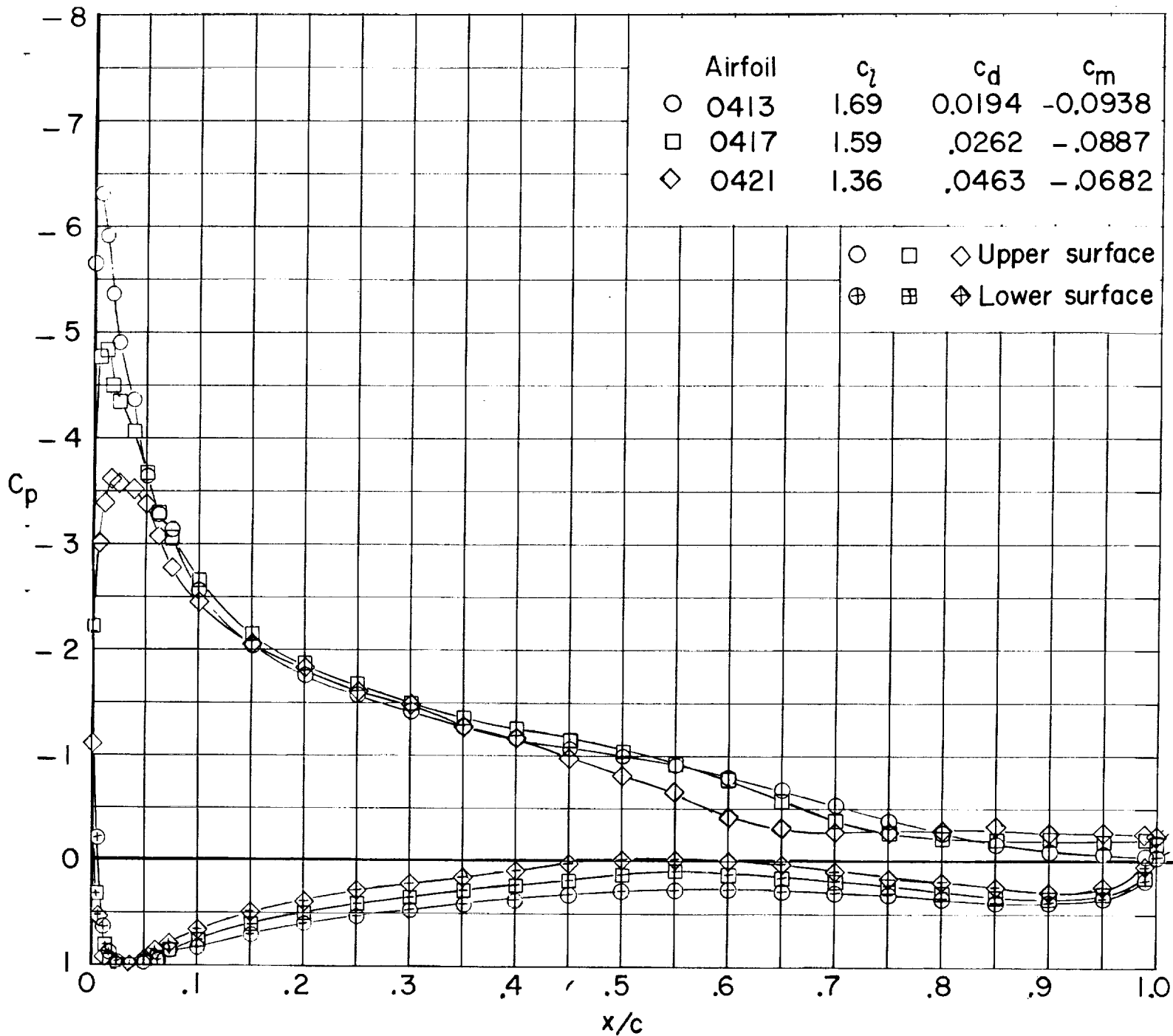
(a) $\alpha \approx 0^\circ$.

Figure 10. - Comparison of chordwise pressure distributions for LS(1)-thickness family of airfoils.
 $R \approx 4.0 \times 10^6$; $M = 0.15$; transition fixed at $x/c = 0.075$. (Flagged symbols indicate base pressure orifice).



(b) $\alpha \approx 6^\circ$.

Figure 10. - Continued.



(c) $\alpha \approx 12^\circ$.

Figure 10. - Concluded.

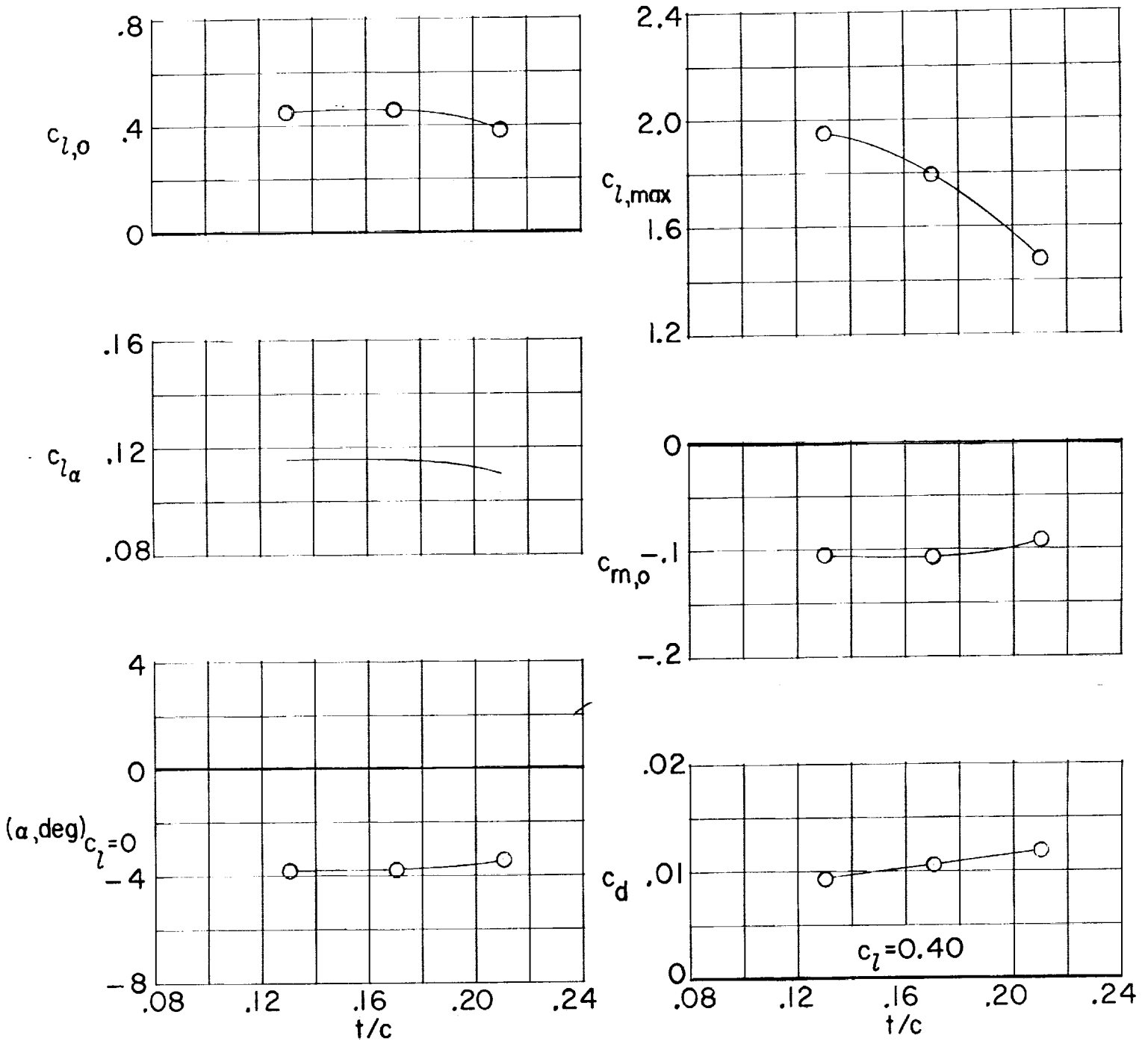


Figure II. - Effect of thickness ratio on section characteristics for LS(1)-thickness family of airfoils.
 $M = 0.15$; $R \approx 4.0 \times 10^6$; transition fixed at $x/c = 0.075$.

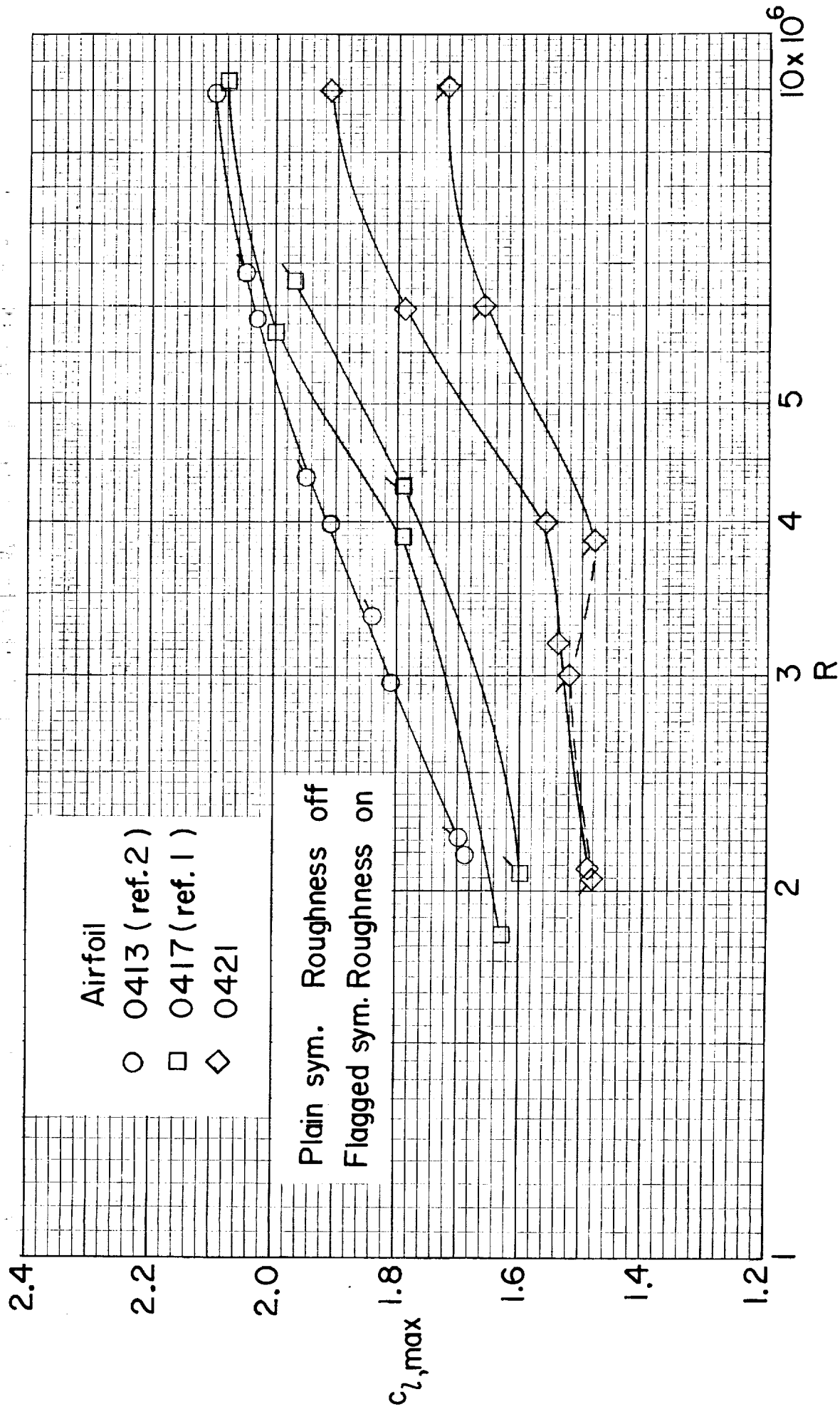


Figure 12.- Variation of maximum lift coefficient with Reynolds number for the LS(I)-thickness family of airfoils. $M = 0.15$.

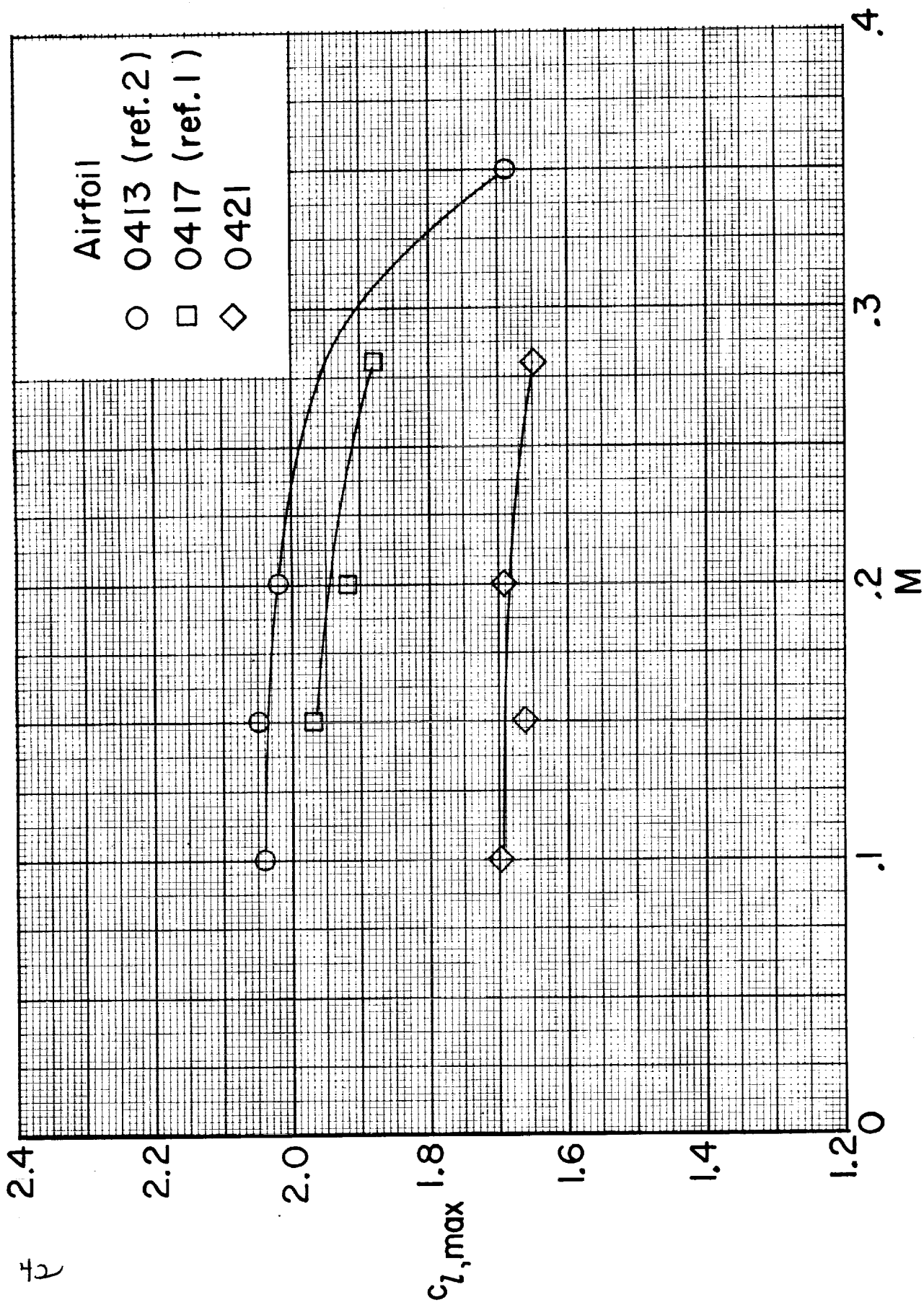
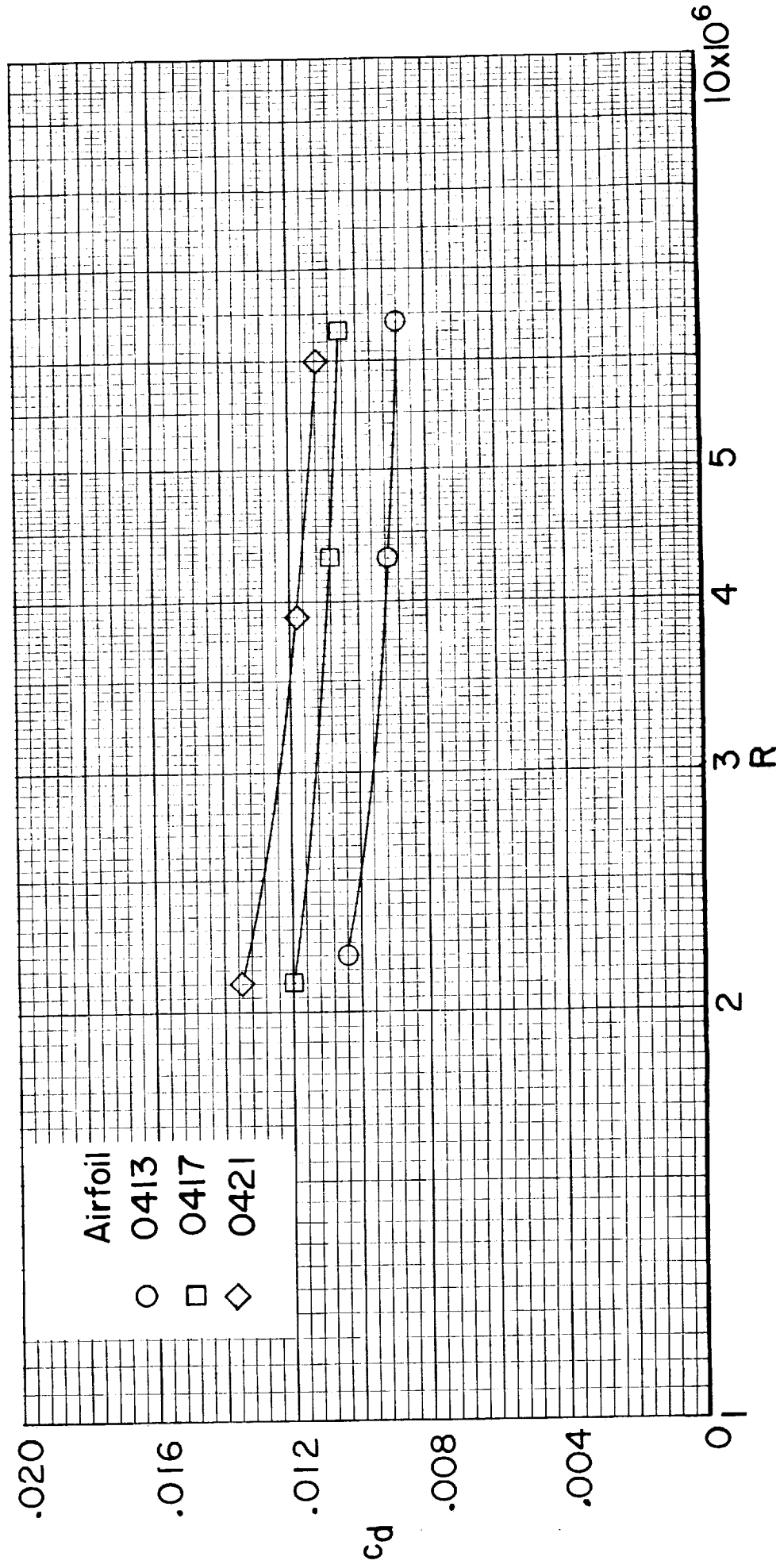
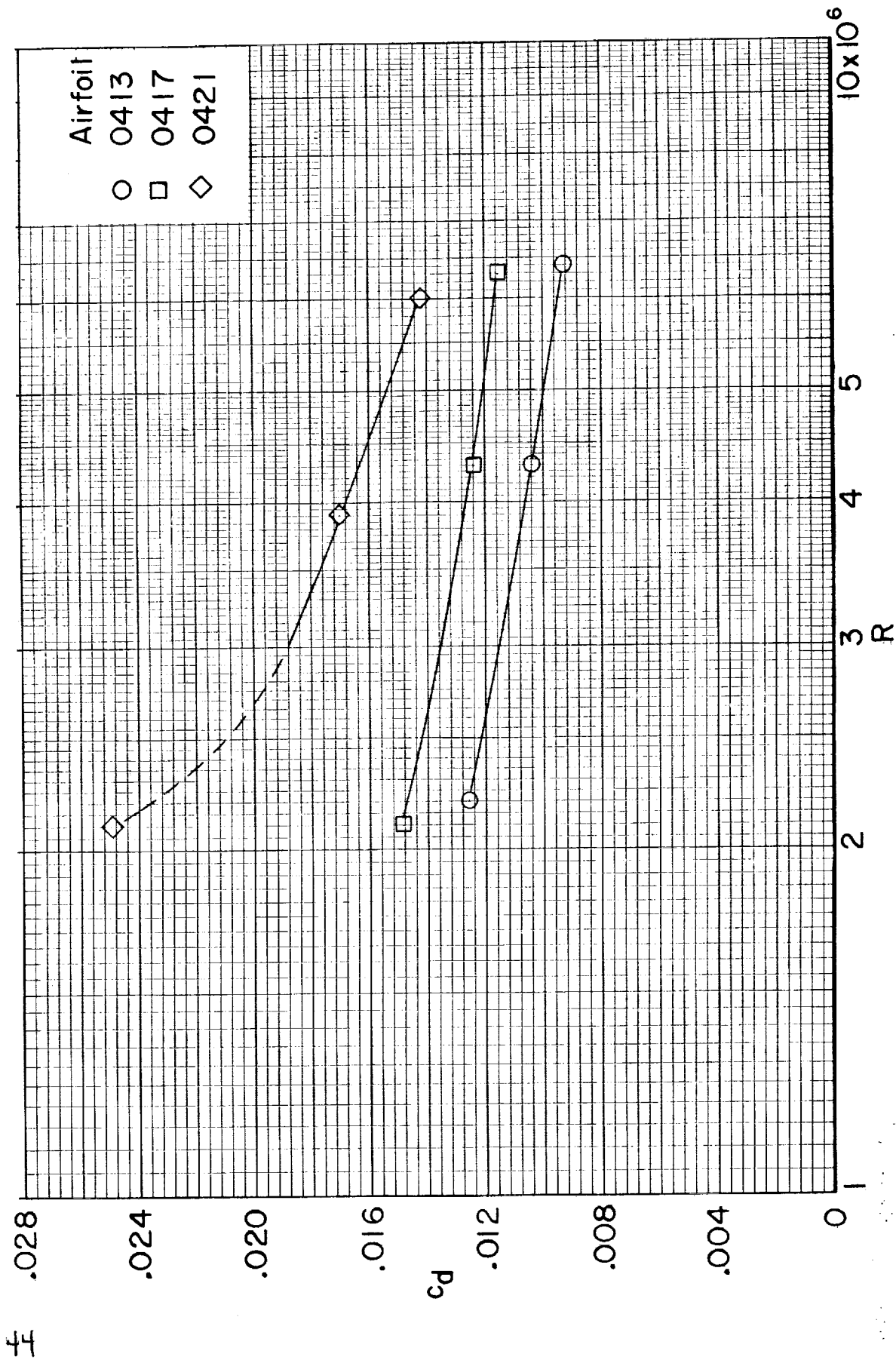


Figure 13. - Variation of maximum lift coefficient with Mach number for LS(1)-thickness family of airfoils. $R \approx 6.0 \times 10^6$; transition fixed at $x/c = 0.075$.



(a) $\zeta = 0.40$.

Figure 14. - Variation of drag coefficient with Reynolds number for LS(1)-thickness family of airfoils. $M = 0.15$; transition fixed at $x/c = 0.075$.



(b) $c_l = 1.0$.

Figure 14. - Concluded.

ORIGINAL PAGE IS
OF POOR QUALITY

Airfoil
—— 0413
- - - 0417
— · — 0421

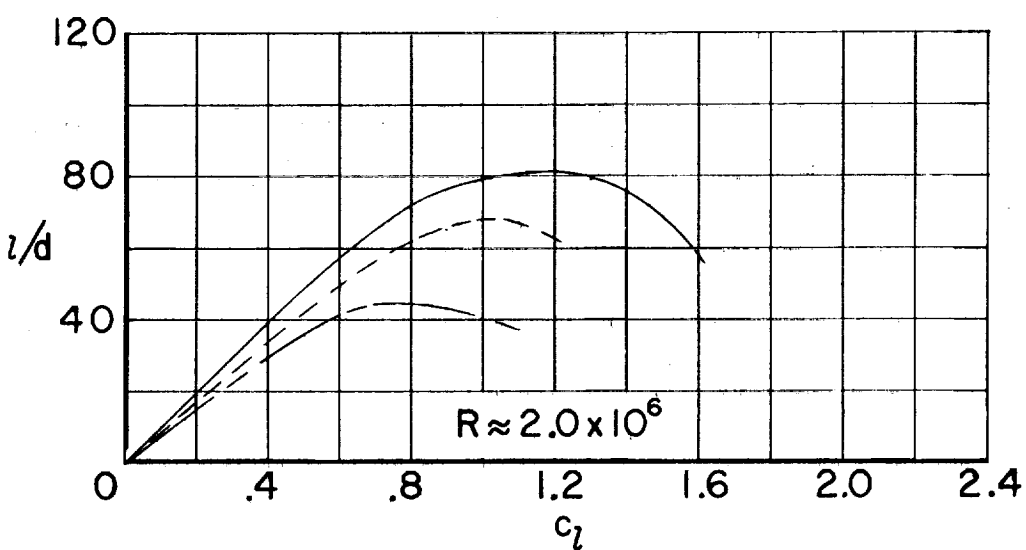
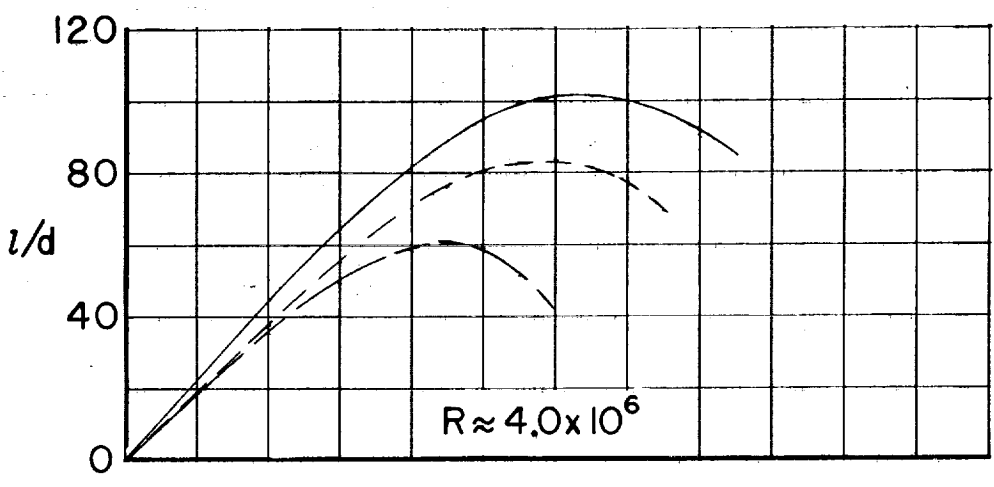
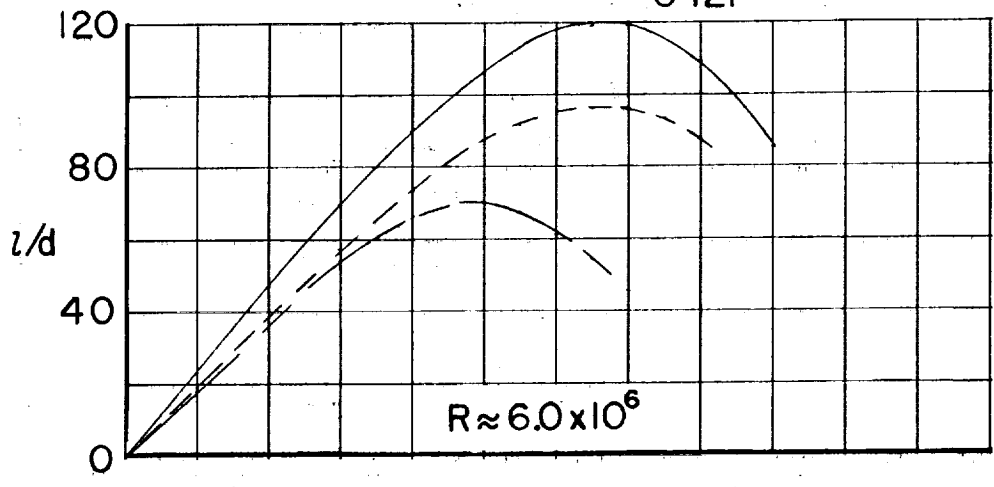


Figure 15. - Variation of lift-drag ratio with lift coefficient for LS(1)-thickness family of airfoils. $M = 0.15$; transition fixed at $x/c = 0.075$.

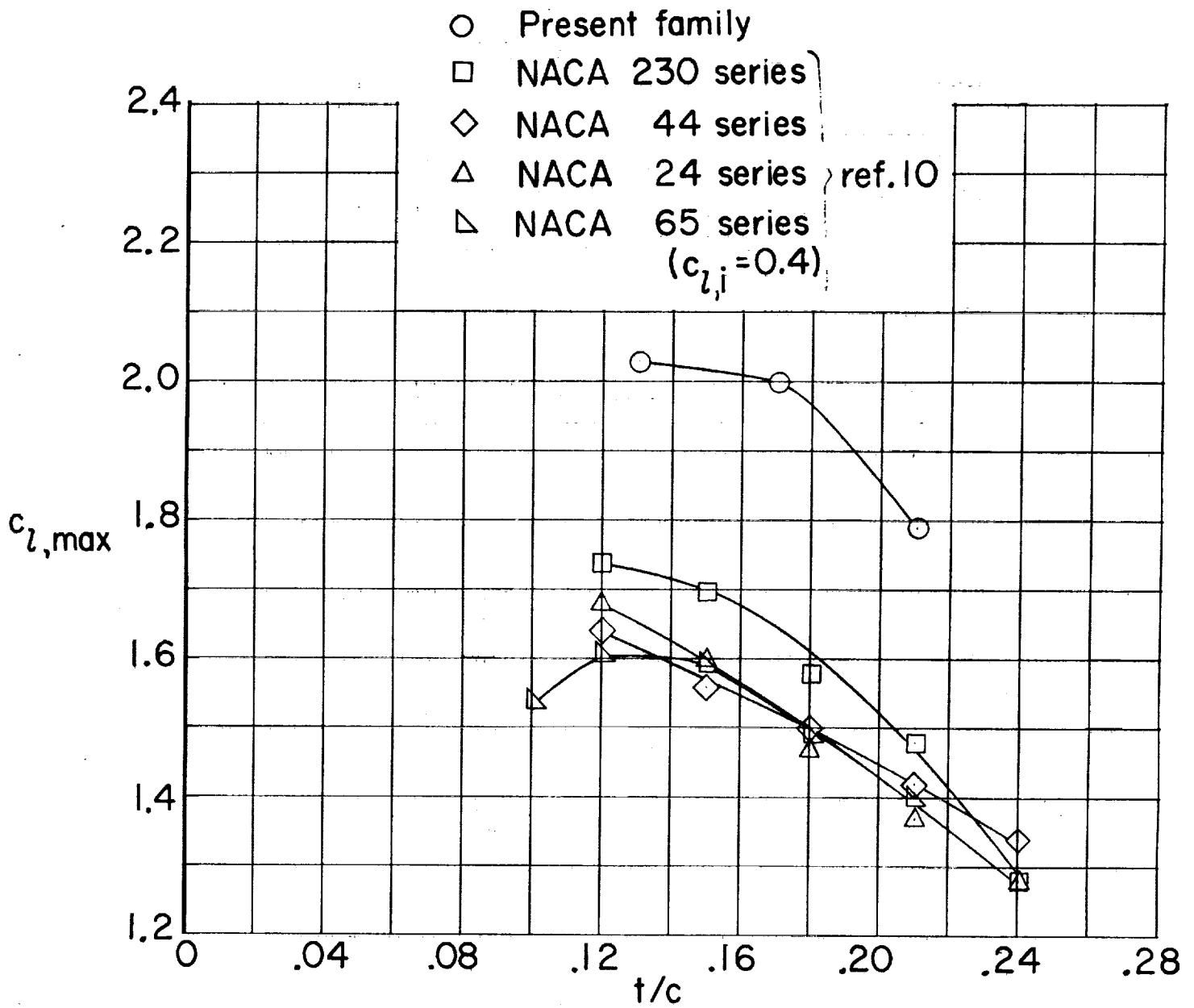
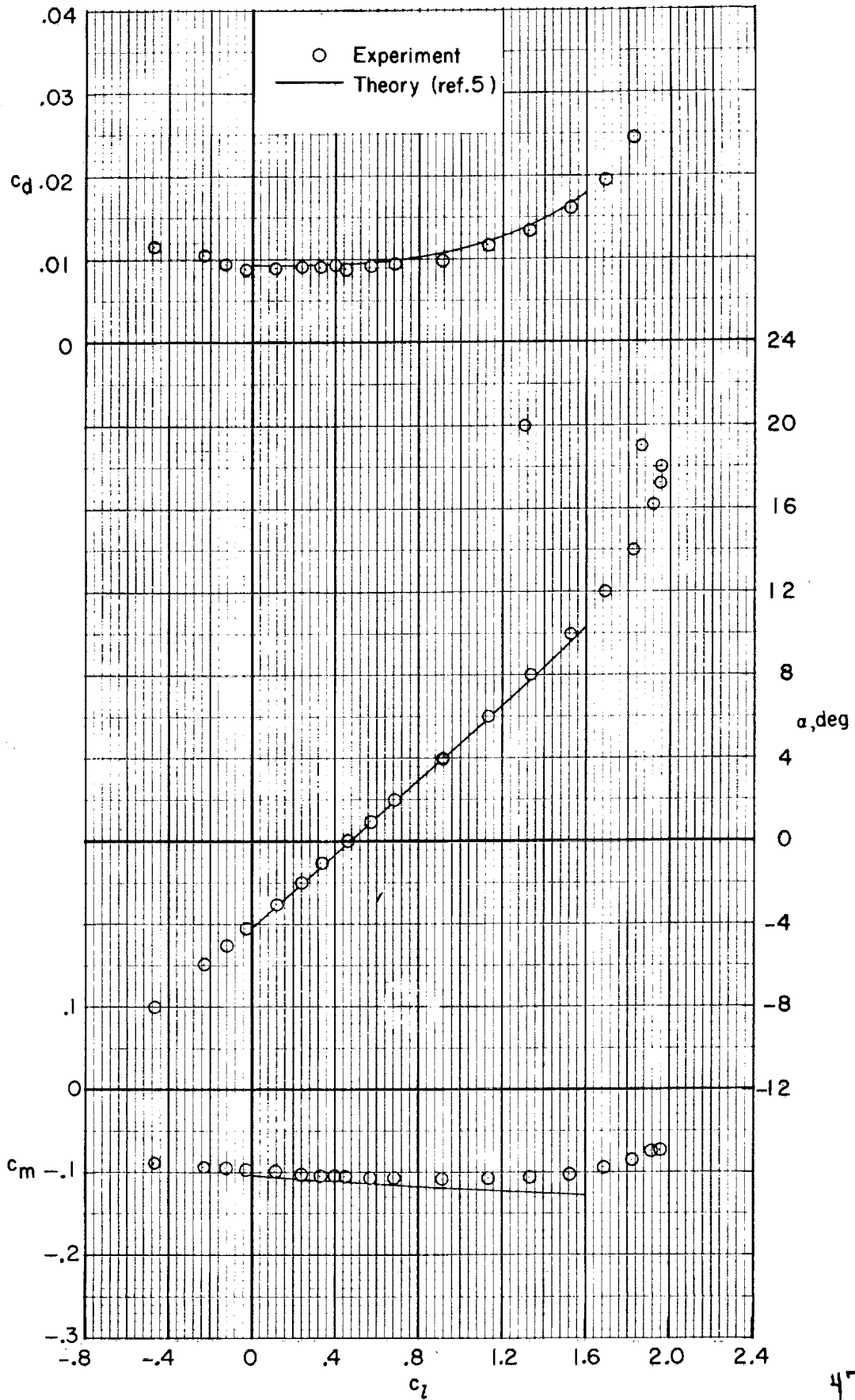
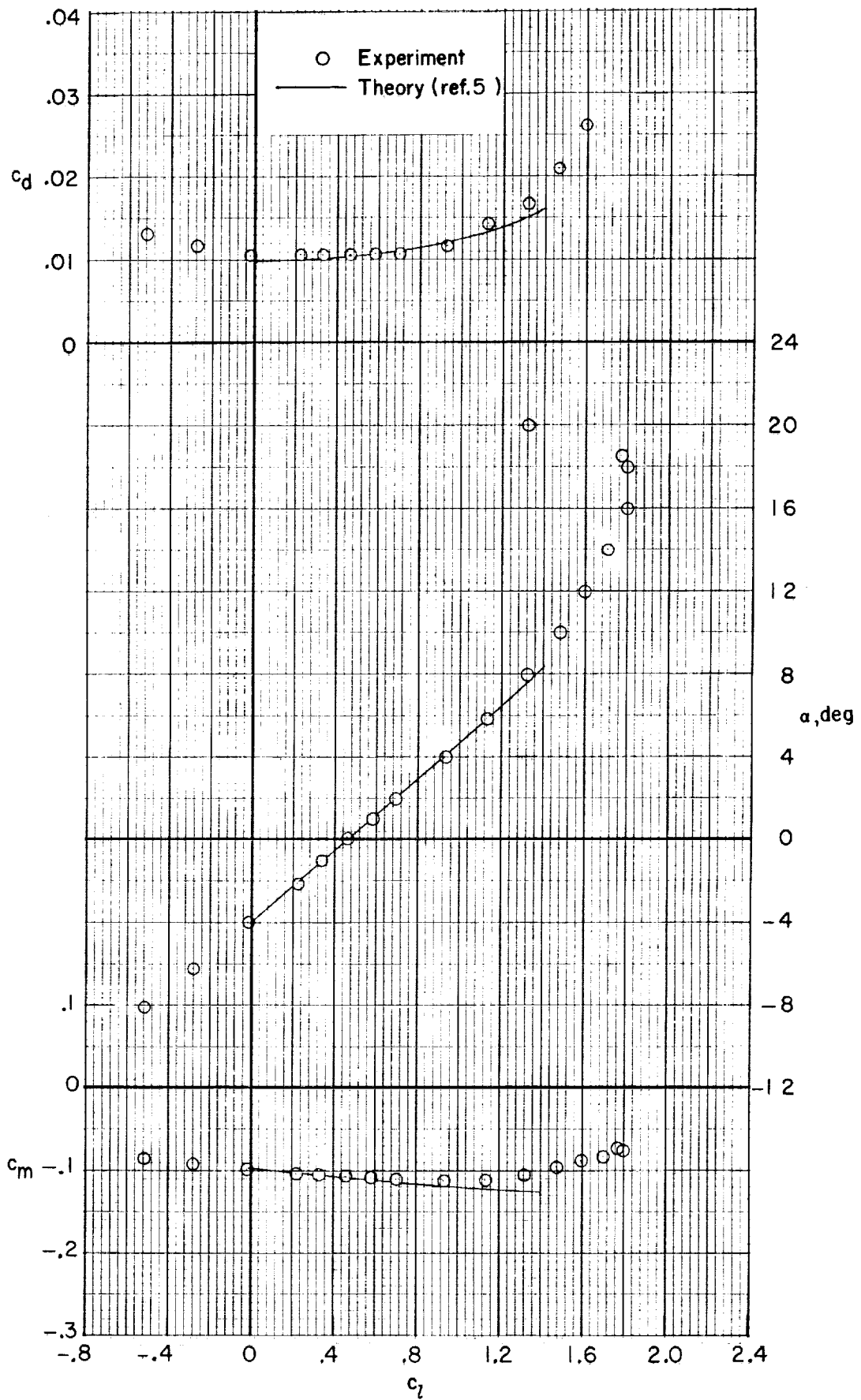


Figure 16. - Comparison of maximum lift coefficient for present LS(1)-thickness family with older NACA airfoils. $R \approx 6.0 \times 10^6$; airfoils smooth; $M \leq 0.17$.



(a) Airfoil 0413.

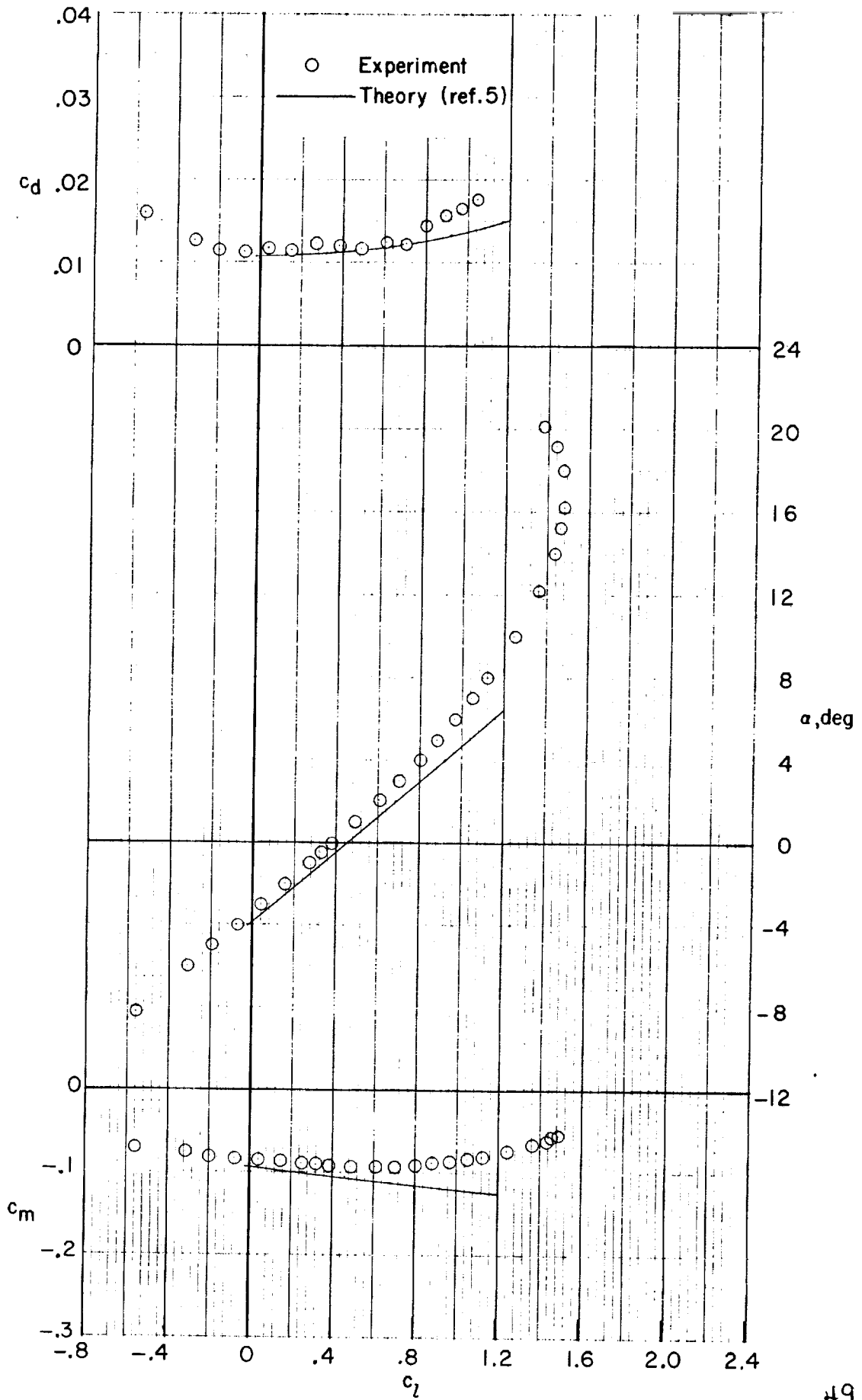
Figure 17. - Comparison of experimental and theoretical section characteristics for LS(1)-thickness family of airfoils. $M = 0.15$; $R \approx 4.0 \times 10^6$; transition fixed at $x/c = 0.075$.



48

(b) Airfoil O417.

Figure 17. - Continued.



(c) Airfoil 0421.

Figure 17. - Concluded.

